A Section 508–conformant HTML version of this article is available at https://doi.org/10.1289/EHP14873.

Neurological Outcomes of Joint Exposure to Polystyrene Micro/Nanospheres and Silver Nanoparticles in Zebrafish

Jie Song,[1] Qian Pu,[1] Chen Chen,[1] Xingcheng Liu,[1] Xinlei Zhang,[1] Zejun Wang,[1] Jin Yan,[1] Xuedong Wang,[1] Huili Wang,[1] and Qiuhui Qian[1]

[1]National and Local Joint Engineering Laboratory of Municipal Sewage Resource Utilization Technology, School of Environmental Science and Engineering, Suzhou University of Science and Technology, Suzhou, China

Background: Micro/nanoplastics and silver nanoparticles (AgNPs) are emerging environmental contaminants widely detected in aquatic environments. However, previous research has primarily focused on the interactions between micro/nanoplastics and organic substances or heavy metals, whereas the interactions and combined toxic effects of micro/nanoplastics with AgNPs remain unclear.

Objective: Our study aimed to investigate the effects and mechanisms of coexposure to AgNPs and polystyrene micro/nanospheres (PS M/NPs) on the nervous system, comparing the toxicity of AgNPs alone and in combination with PS M/NPs in larval zebrafish.

Methods: We investigated the dynamics of AgNPs' (5 nm) adsorption onto PS M/NPs (5 μm/100 nm) using inductively coupled plasma–mass spectrometry. Zebrafish larvae were coexposed to PS M/NPs (200 μg/L) and AgNPs (10 μg/L) from 6 h post fertilization (hpf) to 72 hpf to ∼120 hpf to evaluate neuroinflammatory effects from multiple perspectives, including developmental abnormalities, oxidative stress, neurobehavioral differences, vascular development, immune responses, differences in gene expression, and differences upon neuroinflammation inhibitor addition.

Results: Adsorption experiments showed PS M/NPs could stably adsorb AgNPs, with higher adsorption in smaller particles. Zebrafish larvae exposed to combined PS M/NPs and AgNPs demonstrated neurodevelopmental abnormalities, including developmental malformations, lower levels of locomotor activity, delayed response, and abnormal neuronal development. In addition, exposed zebrafish also exhibited disrupted neurodevelopmental markers, including vascular and apoptotic indicators, and oxidative stress and neuroimmune responses. Quantitative real-time polymerase chain reaction analysis showed differences in gene expression within neurotoxic pathways in PS M/NPs and AgNPs-exposed zebrafish, focusing on key genes in immunity, apoptosis, vascular, and neural development. Furthermore, these neurotoxic effects induced by combined exposure were alleviated following the introduction of the neuroinflammation inhibitor curcumin.

Discussion: Our findings demonstrate that polystyrene nanospheres (PSNPs) intensified AgNPs-induced neurotoxicity in larval zebrafish, whereas polystyrene microspheres (PSMPs) had a lesser effect, indicating distinct gene regulation roles when combined with AgNPs. These findings enhance the assessment of environmental risks in settings with coexisting nanomaterials and microplastics, offering important insights for evaluating combined exposure risks. https://doi.org/10.1289/EHP14873

Introduction

Microplastics, defined as plastic debris with a particle size of <5 mm, have emerged as a significant concern because of their widespread contamination of aquatic environments.[1,2] The production of plastic has reached alarming levels, with over 36,050 million tons being produced worldwide in 2018, and a substantial portion of ∼80,000 tons being released into waterways.[3,4] Furthermore, research indicated that the annual inflow of microplastics into the ocean approach 0.8–23 million tons.[5,6] Concentrations of microplastics in aquatic environments typically range between ng/L and mg/L.[7–9] It has been proved that microplastics can induce neurotoxicity in aquatic organisms by interfering with neural-related enzymes, destructing lipid peroxidation, and producing behavioral abnormalities.[3,10,11] For example, Hamed et al.[12] observed neurotoxic effects in carp exposed to microplastics, leading to neuronal necrosis in the brain. Yu et al.[13] reported that microplastics exposure provoked severe hyperactivity and remarkable variations in neurotransmitters including dopamine (DA), serotonin (5-HT), and the cholinergic system in zebrafish. Numerous studies have provided compelling evidence that the harmful impacts of microplastics pollution may be exacerbated by the combined effects of other environmental contaminants, including organic pollutants,[14] microorganisms,[15] and heavy metals.[16] Recent research indicated that the bioavailability of organic pollutants in the food chain was enhanced through the adsorption of organic contaminants by micro/nanoplastics.[17,18] Microplastics exhibit significant adsorption capabilities toward organic pollutants such as bisphenol A (BPA)[19,20] and triclosan,[21] thereby posing a considerable threat to living organisms and exerting additive effects. In contrast to organic pollutants, heavy metals exhibit a greater propensity for bioaccumulation and are more resistant to degradation, leading to pronounced detrimental effects on various species, including humans.[22] Microplastics, acting as vectors, demonstrate a strong affinity for heavy metals, potentially enhancing their bioavailability and altering their toxicological properties.[23,24] Despite the increasing research on microplastics, there is limited research on the interactions between microplastics and other emerging pollutants.

Silver nanoparticles (AgNPs) represent one of the most ubiquitously employed engineered nanomaterials, gaining particular prominence for their efficacy as disinfectants during the COVID-19 pandemic,[25] thereby heightening concerns regarding environmental contamination.[26] Studies conducted by Xiao et al.[27] reported a broad particle size distribution range of 18.8–41.0 nm for AgNPs in Taihu Lake, China, with the average concentration of 82.8 ± 21.4 ng/L in the water. In the rivers in Malaysia that receive various types of wastewater effluents, the concentration levels of AgNPs have alarmingly escalated to a range between 0.1 and 10 mg/L.[28] The pervasive dispersal of AgNPs within

Address correspondence to Huili Wang. Email: whuili@163.com. And, Qiuhui Qian. Email: qhqian@usts.edu.cn

Supplemental Material is available online (https://doi.org/10.1289/EHP14873).

The authors declare no competing financial interest.

Received 23 February 2024; Revised 4 March 2025; Accepted 20 March 2025; Published 12 May 2025.

aquatic realms posits the potential for bioaccumulation, consequently eliciting deleterious effects on aquatic organisms. An empirical study unveiled that zebrafish, on exposure to AgNPs, manifested signs of neurotoxicity and hepatic toxicity, with subsequent potential ramifications on their offspring's health.[29] Corroborating this, research by Yan et al.[30] ascertained the presence of AgNPs in various organs of medaka fish, including the brain, ovaries, gills, liver, and gut. An intriguing finding was that there was evidence of maternal transfer of AgNPs to the progeny. Moreover, AgNPs have been implicated in compromising the integrity of the blood–brain barrier, blocking the formation of novel neurons, and inducing neurotoxicity in juvenile rats via mechanisms rooted in endoplasmic reticulum stress.[31] However, the underlying mechanism of the neurotoxicity of AgNPs remains unclear. In addition, the complicated environmental behaviors of AgNPs, characterized by aggregation, deposition, accumulation, and bioavailability, invariably sculpt its toxicological profile.

Recent research has revealed that microplastics and artificial nanomaterials permeate the environment via analogous vectors, encompassing medical waste, domestic effluent, and industrial wastewater.[32,33] Notably, during the recent outbreak of COVID-19 pandemic, alongside the degradation processes in the environment, myriad protective products released ecotoxicologically significant micro/nanoplastics, nanoparticles [notably silver (Ag) and copper], and organic contaminants.[34] Consequently, there exists a potential synergy between micro/nanoplastics and AgNPs within their natural milieu. A pivotal study conducted by Li et al.[35] ascertained that polystyrene (PS) possessed the capability to sequester citrate-coated AgNPs from aqueous media as distinct particulate entities, culminating in the formation of AgNPs–PS microplastics complexes. This finding underscored the potential role of microplastics as vehicular agents facilitating the translocation of AgNPs into biotic systems. Nonetheless, the research by Li et al. focused on the interaction between microplastics and AgNPs in aqueous solution and did not evaluate the toxicity of such interactions. Furthermore, Jia et al.[36] documented the concurrent presence of AgNPs (30 nm) and micro/nanoplastics, revealing synergistic toxic effects on ciliates, where the combined toxicity of micro/nanoplastics with AgNPs was more pronounced than individual exposures. Building on the observed coexistence and interactions of micro/nanoplastics and AgNPs in environmental contexts and their demonstrated toxicity toward protozoa, it is hypothesized that the presence of microplastics could potentially modulate the toxic effects of AgNPs on higher vertebrate species.

The central nervous system (CNS) of zebrafish exhibits functional similarity to that of humans. Furthermore, their sensory pathways manifest a significant degree of homology with human systems. Consequently, zebrafish emerge as a representative model for the evaluation of developmental neurotoxicological impacts.[37,38] In this study, zebrafish were used as a model organism, with polystyrene micro/nanospheres (PS M/NPs) representing micro/nanoplastics, to investigate the neurotoxic effects and potential mechanisms triggered by the coexposure of micro/nanoplastics and AgNPs. In addition, we aimed to delineate the comparative toxicity differences in larval zebrafish among AgNPs, AgNPs + polystyrene microspheres (PSMPs), and AgNPs + polystyrene nanospheres (PSNPs), unveiling the molecular mechanisms underlying the neurotoxicity induced by AgNPs under the adsorption of microplastics of varying particle sizes.

Materials and Methods

Reagents

The polyvinylpyrrolidone-coated AgNPs (5 nm, 5 mg/mL, No. NCXSEPE5-25 mL) used in this study were purchased from Sigma-Aldrich. PSMPs (5 μm; No. 86542350) and PSNPs (100 nm; No. 86542301) were obtained from Tesulang Chemical Material Factory. Cy5-labeled PSMPs (5 μm; No. zc-psy-5u) and PSNPs (100 nm; No. zc-psy-100n) were purchased from Jiangsu Zhichuan Technology Co., Ltd. A series of assay kits were acquired from Beijing Solabao Technology Co., Ltd., and TRIzol kits, reverse transcription kits, and quantitative PCR kits were provided by Takara Biotechnology Co. As an applied extension, microspheres (MPs) including polylactic acid (PLA) MPs (5 μm; Jiangsu Zhichuan Technology Co., Ltd.), polyamide (PA) MPs (5 μm; Kaixuan Plastic Technology Co., Ltd.), and PSMPs with mixed particle sizes (1–100 μm; Tesulang Chemical Material Factory) were incorporated into the study. All the other reagents used were of analytical grade.

Characterization of AgNPs and PS M/NPs

The AgNPs stock solution (5 mg/mL) was diluted with deionized water to achieve the corresponding working concentration, followed by ultrasonication at 50 W/L and 50 kHz for 40 min. The ultraviolet–visible spectrophotometry (UV-vis) absorption spectra of AgNPs suspensions (1 mg/L) were obtained using a spectrophotometer (UV-5500PC; Shanghai Yuanxi Instrument Co., Ltd.), with a detection range of 200 to 800 nm. Prior to transmission electron microscopy (TEM) imaging, a 2 μL aliquot of AgNPs (0.05 mg/mL) was drop-cast onto a carbon-coated copper grid and air-dried at room temperature. Then the size and morphology of samples were characterized by TEM (Tecnai G2 spirit Biotwin; FEI), with a high-resolution charge-coupled device (CCD) camera. For morphological characterization of PS M/NPs powder using scanning electron microscopy (SEM; S-4800, Hitachi), the powder was evenly spread onto an aluminum sample holder covered with conductive tape for fixation, followed by gold sputter coating. During imaging, the SEM accelerating voltage was set between 1–5 kV, with the working distance adjusted to 5–15 mm. The average hydrodynamic diameter of AgNPs (0.05 mg/mL) and PS M/NPs (1 mg/mL), as well as the zeta potential of AgNPs (0.05 mg/mL), were analyzed using dynamic light scattering (DLS) with a Zetasizer instrument (Malvern) at a measurement temperature of 25° and a scattering angle of 90°, comprising triplicate samples with triplicate measurements for each.

Zebrafish Maintenance and Exposure Protocols

Wild-type zebrafish (AB strain) and three transgenic zebrafish lines—Tg(*elavl3*:EGFP), Tg(*kdrl*:mCherry), and Tg(*coro1a*:EGFP)—were purchased from the Chinese Zebrafish Resource Center. The transgenic Tg(*elavl3*:EGFP) line, whose neurodevelopmental marker gene *elavl3* is labeled with enhanced green fluorescent protein (EGFP), enables the specific labeling of neurons throughout the organism.[39] The Tg(*kdrl*:mCherry) line, whose vascular endothelial growth factor receptor gene *kdrl* is labeled with mCherry, specifically marks epithelial cells.[40] In the Tg(*coro1a*:EGFP) line, both macrophages and neutrophils are labeled by EGFP.[41] The zebrafish were housed under controlled conditions, with the water temperature set at 28 ± 1°C and the pH kept between 6.8 and 7.5. They were exposed to a 14-h light period followed by 10 h of darkness. Adult zebrafish were fed twice daily with a diet of freshly hatched brine shrimp. The night before the experiment, eight adult zebrafish (1:1 male-to-female ratio) were randomly selected from each tank and placed in 2-L breeding tanks with dividers. The tanks were kept dark until the next morning when lights were turned on to trigger spawning. Embryos were then collected using a fine mesh, transferred to petri dishes with ultrapure water. For the exposure experiments, zebrafish embryos [6 h post fertilization (hpf)] were randomly assigned to 100 mm diameter petri

dishes containing the corresponding exposure solutions, with 60 embryos per group. The dishes were placed in an incubator maintained at 28°C for the designated exposure duration, as required for subsequent experiments. The sample sizes and exposure durations necessary for the corresponding end point measurements are listed in Table S1. Except for the transgenic zebrafish observations, all other experiments were conducted using the AB wild-type zebrafish strain. All experimental procedures involving embryos and larval zebrafish were executed in rigorous compliance with the stipulations set forth by the Institutional Animal Care and Use Committee guidelines.

Acute Exposure Assessment of AgNPs

For acute toxicity assessment of AgNPs, we established six exposure concentrations: 0, 25, 50, 75, 100, and 150 μg/L. The AgNPs' stock solution underwent 30-min ultrasonic dispersion before application. Zebrafish embryos were exposed to a series of AgNPs exposure solutions prepared with ultrapure water in six-well plates with 4 mL per well. The exposure solutions were refreshed daily. Fresh AgNPs exposure solutions were prepared every 24 h to ensure consistent exposure. Heartbeat cessation was deemed the mortality end point. Deceased embryos were promptly catalogued, and after 96 h of exposure, median lethal concentrations (LC_{50}) were determined. Each group comprised three replicates with 30 embryos per group.

No-Observed-Effect Concentration of PS M/NPs

For preparation, PS M/NPs were solubilized in ultrapure water, achieving a concentration of 5 mg/mL. Subsequent to this, the particulates underwent a 60-min ultrasonic dispersion to ensure uniformity. A dedicated stock solution of the M/NPs was replenished weekly. Zebrafish embryos were exposed in six-well plates (4 mL per well) to concentrations of 0, 10, 20, 40, 80, and 160 mg/L. Each experimental cohort consisted of three replicates, each housing 30 embryos. Observational assessments, focusing on malformations and hatching rates, were meticulously conducted at 96 hpf under PS M/NPs exposure.

Interaction between AgNPs and PS M/NPs

The study on the interactions between AgNPs and PS M/NPs was conducted in a manner similar to that of previous research.[35] The cited study provided a detailed account of the key steps of investigating the binding efficiency between AgNPs and microplastics. In this study, the following modification was implemented: prior to testing, membrane filtration was applied to remove PS M/NPs. This step was essential to ensure the accuracy of the experimental results, because the smaller particle size of the MPs in the experiment caused them to remain suspended in the liquid, potentially interfering with detection outcomes. The specific experimental procedure was outlined as follows: A suspension of PS M/NPs was meticulously prepared in ultrapure water at a concentration of 10 g/L. To ensure homogeneous dispersion of the MPs, the suspensions underwent a 30-min ultrasonic treatment. These were then subjected to a 24-h dark incubation with stirring at 200 rpm. Subsequently, an AgNPs solution or standard solution of Ag^+ was introduced into the container until achieving a 10-mg/L concentration. This mixture was maintained under dark conditions at ambient temperature, with a stirring rate of 150 rpm for a week. At predetermined time points (0 min, 5 min, 10 min, 30 min, 1 h, 6 h, 12 h, 24 h, 48 h, 72 h, and 168 h), 2.5-mL samples were taken from the amber glass bottles using a pipette and immediately filtered through anodic aluminum oxide (AAO) inorganic membrane filters (0.22 μm; Sigma-Aldrich) to remove PS M/NPs. A 0.5-mL fraction of the resultant filtrate underwent digestion in 70% nitric acid for 2 h at 60°C, facilitating the quantification of the concentrations of AgNPs or Ag^+ via inductively coupled plasma–mass spectrometry (ICP-MS; Agilent 7500cx). Concurrently, UV-vis spectroscopy (UV-5500PC; Shanghai Yuanxi Instrument Co., Ltd.) captured the absorbance of filtrate, with the wavelength range set to 300–800 nm and a scanning speed of 1 nm/s. After a 168-h incubation, a 1-μL sample of the suspensions was directly taken (without filtration) using a micropipette and deposited onto a carbon-coated copper grid for TEM observation. Each experimental set was triply replicated ($n = 3$). The binding efficiency of PS M/NPs with AgNPs was deduced using the subsequent equation:

$$R_t = \frac{(C_0 - C_t)}{C_0} \times 100\%. \tag{1}$$

R_t (%) represents the percentage removal efficiency of AgNPs by PS M/NPs at the designated sampling time, with C_0 and C_t denoting the initial and time-specific concentrations of AgNPs in the suspension (mg/L), respectively.

The adsorption rate of AgNPs by PS M/NPs was calculated using the following equation:

$$q_t = \frac{(C_0 - C_t) \times V}{W}, \tag{2}$$

where q_t (mg/g) is the quantity of AgNPs adsorbed at a given sampling interval, C_0 and C_t represent the initial and sampled concentrations of AgNPs in suspension (mg/L), respectively. V and W correspond to the volume of AgNPs solution (L) and the mass of M/NPs (g), respectively.

For a nuanced interpretation of the adsorption dynamics, both pseudo-first and pseudo-second order kinetic models were employed to model the potential adsorption pathways. The respective linear formulations for these models are provided as follows:

$$\ln(q_e - q_t) = \ln q_e - k_1 t \tag{3}$$

and

$$\frac{t}{q_t} = \frac{1}{k_2 q_e^2} + \frac{t}{q_e}, \tag{4}$$

where q_e (mg/g) and q_t (mg/g) signify the amount of AgNPs adsorbed on the M/NPs at equilibrium and sampling time t, respectively; t denotes the exposure time (min), and k_1 (per minute) and k_2 (g/mg/min) are the rate constant of the pseudo-first order model and pseudo-second order model.

Developmental Toxicity of Combined Exposure of AgNPs and PS M/NPs to Zebrafish Larvae

Based on the above the no-observed-effect concentration (NOEC) of PS M/NPs (10 mg/L) and a relevant publication,[42] we chose a concentration of 200 μg/L PS M/NPs to simulate microplastics contamination in natural waters. Drawing from the identified LC_{50} of AgNPs and relevant environmental data, the exposure concentration was set at 10 μg/L for AgNPs. Both M/NPs and AgNPs stock solutions were sonicated for 40 min, subsequently mixed in proper proportions, and allowed a 20-min equilibration to ensure adequate interactions. Healthy embryos (6 hpf) were selected under a microscope and randomly distributed into 100 mm diameter petri dishes. Each dish contained 60 embryos and 40 mL of exposure solution, and the dishes were placed in an incubator at 28°C. These embryos were categorized into six distinct groups: control, AgNPs, AgNPs+PSNPs (AN), AgNPs+PSMPs (AM),

PSNPs, and PSMPs. Each group incorporated three replicates, each containing 30 embryos. The exposure solution was refreshed every 24 h, with zebrafish morphological differences observed and recorded. Tic frequency was assessed at 24 hpf, hatching and heart rate were evaluated at 48 hpf, and body length was measured at 96 hpf.

Determination of Acetylcholinesterase and Oxidative Stress–Related Indicators

After 96 hpf exposure to AgNPs, embryos were randomly collected and homogenized on ice to determine the levels of acetylcholinesterase (AChE) and three indicators of oxidative stress, glutathione reductase (GSH), and the lipid peroxidation product malondialdehyde (MDA), as well as the accumulation of reactive oxygen species (ROS). Biochemical assays targeting AChE, GSH, and MDA were executed using commercial kits (S-002; S-005; S-010; Solarbio), adhering strictly to the manufacturer's protocol. For each assay, 30 larvae were randomly selected from the exposed group of 60 as one biological replicate. Three biological replicates were used, and each biological replicate was measured in triplicate. Analysis was facilitated by a Thermo Scientific Varioskan LUX Multimode Microplate Reader, with parameters strictly set according to the instructions provided in the respective assay kit. The "Absorbance" mode was selected, and the corresponding wavelengths were configured (AChE: 412 nm; GSH: 405 nm; MDA: 532 nm, 600 nm) per the kit's guidelines. A 96-well plate was used, with each well containing 100–200 μL, and the reading time adjusted to meet the assay requirements.

To assess ROS levels under combined exposure, 12 larvae were randomly selected from each group following exposure from 6 hpf to 120 hpf. The larvae were rinsed with phosphate-buffered saline (PBS) and transferred to a 6-well plate, with 4 mL of buffer containing 2′,7′-dichlorodihydrofluorescein diacetate (DCFH-DA) added to each well for staining. After incubating in the dark at 28.5°C for 30 min, the larvae were gently rinsed with PBS to remove excess dye. Subsequently, they were anesthetized in 0.04% MS-222 for 2–5 min and immediately visualized ($\lambda_{ex} = 488$ nm; $\lambda_{em} = 525$ nm) under a fluorescence-equipped upright microscope Eclipse Ci-L (Nikon). Fluorescence intensities across groups were subsequently quantified using ImageJ software.

Behavioral Assays

Behavioral assessments of 120 hpf zebrafish larvae post combined exposure were conducted employing EthoVision XT software (Noldus IT). These evaluations incorporated voluntary movements, turning behaviors, responses to light–dark transitions, and auditory stimuli. All behavioral experiments with zebrafish larvae were conducted in sterile 96-well plates. After exposure from 6 hpf to 120 hpf, 30 well-developed larvae from each treatment group were transferred to the 96-well plate (one larva per well), with 200 μL of ultrapure water added to each well. The temperature was maintained at 28 ± 1°C. Experimental time was strictly controlled between 0900 hours (9:00 A.M.) and 1400 hours (2:00 P.M.). Video recordings and data analysis were performed using EthoVision XT software (Noldus IT). The experimental protocols were meticulously adhered to specific criteria, and the resultant data were analyzed in alignment with established methodologies previously adopted by our research group.[43] Each treatment group underwent three technical replicates and three biological replicates.

Spontaneous swimming behavior of larvae. After a 5-min acclimation period (excluded from analysis), the spontaneous swimming activity of zebrafish larvae was observed. Swimming trajectories were recorded for 5 min using EthoVision XT software, which subsequently analyzed and calculated the total distance moved and swimming velocity.

Larval turning angle test. After a 5-min dark adaptation period (excluded from analysis), the differences in turning angles of larvae in each group were observed for 20 min to assess behavioral anxiety. EthoVision XT software was used to record the changes in turning angles every minute.

Light–dark cycle experiment. After a 10-min dark adaptation period (excluded from analysis), the light–dark cycle was set at 10 min of light followed by 10 min of darkness, repeated for two cycles. EthoVision XT software was used to record the locomotor activity of zebrafish larvae during both the light and dark phases, and the distance moved per minute was calculated.

Larval acoustic startle response test. After a 5-min adaptation period (excluded from analysis), the behavioral responses of larval zebrafish were recorded for 9 min using EthoVision XT software, with a sound stimulus applied at the 3-min mark at level 8. The average swimming speed was calculated as an indicator of the larval response to the acoustic stimulus.

Touch Reaction Assay

Tactile stimuli, applied by touching the zebrafish, instinctively trigger escape responses. These stimuli are commonly used to elicit startle reactions or directional swimming, providing insights into neural circuitry, motor coordination, and sensory integration.[44] After exposure from 6 hpf to 96 hpf, 10 larvae from each group were selected for individual experiments. Each larva was gently transferred using a pipette into a $2 \times 2 \times 1$ cm acrylic container with a total solution volume of 1 mL. The movement behavior of larvae was recorded for 1 s following tactile stimulation using an Olympus SZX16 high-speed camera. Video frames were extracted at 0.1-s intervals using QuickTime Player software (Apple Macintosh, ver. 7.79.80.95) to capture movement at different time points.

Observation of Combined Exposure to Transgenic Zebrafish

To comprehensively assess the developmental toxicity arising from combined exposure, three transgenic zebrafish lines [Tg (*elavl3*:EGFP), Tg(*kdrl*:mCherry), and Tg(*coro1a*:EGFP)] were employed. A total of 24-hpf embryos were observed under a fluorescence microscope to screen for transgenic zebrafish individuals exhibiting a positive phenotype. In each experimental group, 30 fertilized transgenic zebrafish embryos were distributed into six-well plates and subjected to exposure (Control, AgNPs, AM, AN, PSMPs, and PSNPs) until 120 hpf, with the presence of 0.5% N-phenylthiourea (PTU; >98%; P7629, Sigma-Aldrich) to prevent pigmentation. Three independent replicates were performed for each treatment group. Subsequently, transgenic larvae were evaluated at 120 hpf. Ten larval zebrafish were randomly selected from each well and subjected to observation and imaging (EGFP: $\lambda_{ex} = 488$ nm/$\lambda_{em} = 511$ nm; mCherry: $\lambda_{ex} = 587$ nm/$\lambda_{em} = 610$ nm) under an Olympus fluorescence microscope located in Tokyo, Japan. All images were captured at the same magnification, and fluorescence intensity quantification was conducted using Image J software.

AO Apoptosis and Neutral Red Staining

For apoptosis analysis, larval zebrafish were subjected to various treatments (Control, AgNPs, AM, AN, PSMPs, and PSNPs) from 6 hpf to 72 hpf. Subsequently, 15 larvae from each group were placed into a 6-well plate and incubated for 20 min at room temperature with acridine orange/ethidium bromide (AO/EB; Yuanye Bio-Technology Co.). After gently rinsing with PBS to remove any unbound dye, larval zebrafish were anesthetized using 0.04%

MS-222 and then observed ($\lambda_{ex} = 488$ nm, $\lambda_{em} = 515$ nm) under a fluorescence-equipped upright microscope Eclipse Ci-L (Nikon). After imaging, the data were processed and analyzed using ImageJ software.

In the case of neutral red staining, subsequent to different exposures (Control, AgNPs, AM, AN, PSMPs, and PSNPs) from 6 hpf until 72 hpf, each group consisting of 15 larvae was placed in a 6-well plate and incubated with a 2.5 mg/mL solution of neutral red dye (Aladdin) for 6 h at 28.5°C in darkness. Following dye absorption, the zebrafish were anesthetized using 0.04% MS-222, then observed under an upright microscope Eclipse Ci-L (Nikon) and photographed. The enumeration of macrophages was performed automatically using Image J software.

qPCR Assay

Total RNA was extracted from 50 larval zebrafish (per group) using TRIzol reagent, following the manufacturer's prescribed protocols. The concentration of RNA samples was measured using UV/visible nano-spectrophotometer of ScanDrop 250 (Analytik Jena AG), and purity was assessed by the OD_{260}/OD_{280} ratio, the value of which ranged from 1.8 to 2.0, indicating high purity of RNA. Then the reverse transcription of RNA into cDNA was carried out in accordance with the instructions from the Takara reverse transcription kit (Takara Bio Inc.). The process involved cDNA synthesis at 37°C for 15 min, with a subsequent heat inactivation step at 85°C for 5 min. Quantitative real-time polymerase chain reaction (qPCR) was performed under the following cycling conditions: an initial denaturation at 95°C for 30 s, followed by 40 cycles of 95°C for 15 s and 60°C for 30 s, with an additional data acquisition step lasting 15 s at the optimal acquisition temperature. The ABI 7500 Real-time PCR System (Thermo Fisher Scientific, Inc.) was used for detection, with β-actin employed as an endogenous reference gene. The primer sequences (Shangon Biotech) employed for qPCR are provided in Table S2. All qPCR assays were conducted with rigor, comprising three distinct biological replicates, each encompassing three technical replicates. The interpolated cycle threshold (Ct) values, which reached a set threshold above the background noise, served to quantify amplification. The relative expression levels of the target genes were then calculated by employing the $2^{-\Delta\Delta Ct}$ method.

Dissolution Measurements of AgNPs

The dissolution of AgNPs, both in the presence and absence of PS M/NPs, was assessed using 50-mL amber glass bottles, with the released Ag^+ quantified via ICP-MS. Prior to ICP-MS analysis, aliquots of AgNPs suspensions were collected at specific time intervals and subjected to centrifugation through a 3-kDa molecular weight cutoff centrifugal ultrafilter at 8,000 × *g* for 15 min to separate AgNPs.

The Uptake of PS M/NPs by Zebrafish Embryo and Larvae

Zebrafish at 6 hpf were exposed to a solution containing Cy5-labeled PS M/NPs (1 mg/L). The exposure solution was refreshed every 24 h, and observations and imaging were conducted at 24, 72, and 120 hpf by using an inverted fluorescence microscope (IX73, Olympus; $\lambda_{ex} = 640$ nm/$\lambda_{em} = 670$ nm). Subsequently, further quantitative analysis of fluorescence intensity was conducted using Image J software.

Evaluation of Combined Effects

To assess the combined effects of AgNPs and PS M/NPs, the impact of their interactions on the levels of each biomarker was determined using the following equation[45]:

$$Ratio = \frac{effect(AgNPs + PSM/NPs)}{effect(AgNPs) + effect(PSM/NPs) - effect(Control)}, \quad (5)$$

where the effect (AgNPs), effect (PS M/NPs), effect (AgNPs+PS M/NPs), and effect (Control) in Equation (5) refer to the biomarker levels observed in the respective groups. The Mann-Whitney test was employed to assess the difference between the biomarker levels resulting from coexposure of AgNPs and PS M/NPs and those predicted by the sum of the biomarker levels from individual exposure. The type of the interaction of AgNPs and PS M/NPs was defined as follows: *a*) suppressive effect: $p < 0.05$ and the ratio <1; *b*) additive effect: $p > 0.05$; *c*) synergistic effect: $p > 0.05$ and the ratio >1.

Statistical Analyses

Table S1 provides an enumeration of the biological replicates, technical replicates, and the number of zebrafish specimens used at different stages of the biological experiment. All experimental data were meticulously documented and were reported as mean ± standard deviation (SD). Unless otherwise noted, statistical analyses were conducted using one-way analysis of variance (ANOVA) followed by Tukey's multiple comparison test, and the significance levels were denoted as follows: $p < 0.05$ (*), $p < 0.01$ (**) or $p < 0.01$ (***). These statistical analyses were performed employing SPSS 18.0 software (IBM, Inc.).

Results

Characterization of AgNPs and PS M/NPs

Before conducting the toxicity experiments, we undertook an exhaustive characterization of the physicochemical properties of AgNPs by employing TEM and DLS measurements. The TEM analysis unveiled the spherical morphology of AgNPs, revealing an average particle size of 5.18 nm (Figure S1A). In Figure S1B, DLS data showed a uniform particle size of 5.68 nm with a zeta potential of -17.7 ± 1.8 mV, indicating that AgNPs exhibited monodispersity in aqueous solution. UV-vis spectroscopy identified a peak absorption at 410 nm (Figure S1C). For acute toxicity testing, the LC_{50} of AgNPs in larval zebrafish was determined to be 45.76 μg/L (Figure S1D).

The morphology of PS M/NPs was analyzed using SEM and DLS. SEM images (Figure S1E, G) showed that PSNPs and PSMPs were spherical, with average sizes of 73.04 nm and 4.31 μm, respectively, aligning with DLS results [PSNPs: 70.59 nm with polydispersity index (PDI) of 0.574; PSMPs: 4.4 μm with PDI of 0.334; Figure S1F, H]. This finding indicated PSMPs had better dispersion and stability in water than PSNPs.

Determination of NOEC of PS M/NPs in Larval Zebrafish

To ascertain the NOEC of PS M/NPs in zebrafish, larval zebrafish were exposed to varying concentrations of PS M/NPs from 6 hpf to 96 hpf, with no mortality observed throughout the exposure period. In addition, the effects on hatching rates and developmental deformities were assessed. At concentrations above 40 mg/L of PSNPs, larvae exhibited yolk sac edema (Figure S2A), and at 80 mg/L, signs of pericardial edema and spinal curvature were observed. Exposure to 160 mg/L resulted in shortened body length, larger pericardial edema, and developmental delays. Similar deformities were also noted following exposure to PSMPs (Figure S2D). Quantitative analysis of the malformation rate at 96 hpf (Figure S2B,E) showed that PSNPs (≥20 mg/L) and PSMPs (≥40 mg/L) had significantly higher malformation rates in comparison with the control group ($p < 0.01$, $p < 0.001$). Furthermore, the hatching rate in the PSMPs (80 mg/L) group was significantly lower than that of the control

group (Figure S2F, $p < 0.05$), whereas in the PSNPs group, the hatching rate decreased with increasing concentrations, with the 40 mg/L group exhibiting significantly lower hatching rate in comparison with the control (Figure S2C, $p < 0.05$). Based on the observed deformities and hatching rate, the NOEC for PS M/NPs in zebrafish larvae was determined to be <20 mg/L.

Interaction of PS M/NPs with AgNPs

Because AgNPs and microplastics coexisted in the environment, we conducted a comparative analysis of the interaction between AgNPs and PS M/NPs in ultrapure water by monitoring the adsorption process. UV-visible spectral analysis of the AgNPs adsorption onto PSNPs showed a consistent decrease in absorbance at λ_{max} over 72 h, without a shift in λ_{max} (Figure 1A-a). In contrast, PSMPs demonstrated a gradual absorbance reduction at λ_{max}, stabilizing at $\sim$0.2 after 168 h, accompanied by a noticeable red shift in λ_{max} (Figure 1A-b), indicating lesser interaction with AgNPs in comparison with PSNPs. This suggested that larger particle-sized microplastics had a stronger adsorption capacity for AgNPs. TEM observations of the PS M/NPs-AgNPs complexes post 168-h adsorption revealed efficient AgNPs adsorption on PSNPs with minimal residuals (Figure 1B-a), whereas PSMPs showed weaker interaction, leaving significant residual AgNPs (Figure 1B-b).

To thoroughly evaluate the interaction between PS M/NPs and AgNPs, we measured the residual AgNPs concentrations post adsorption at different intervals using ICP-MS. As shown in Figure 1C, PSNPs achieved an adsorption equilibrium at 72 h, with a final removal rate of 98.59% by 168 h. Conversely, PSMPs had a lower final removal rate of 76.67% at the same time frame, indicating the greater efficacy of PSNPs in AgNPs adsorption. When Ag^+ replaced AgNPs, its concentration remained relatively stable throughout the experimental period, suggesting no significant interaction between Ag^+ and PS M/NPs. We further analyzed the adsorption kinetics using pseudo-first order and pseudo-second order models (Figure 1D). For PSNPs, the pseudo-second order model yielded a closer approximation to the experimental q_e value (0.95989 mg/g vs. 0.98591 mg/g) than the pseudo-first order model. Similarly, for PSMPs, the q_e value from the pseudo-second order model (0.6774 mg/g) was closer to the experimental value (0.75674 mg/g) than that from the pseudo-first order model. These results highlighted that the pseudo-second order model provides a superior fit in describing the adsorption process for both groups.

Developmental Toxicity of Combined Exposure to Zebrafish Larvae

After combined exposure of AgNPs and PS M/NPs from 6 to 96 hpf, a series of apparent indexes in larval zebrafish were recorded, including the malformation symptoms, hatching and heart rates, twitch frequency, and body length. Figure 2A revealed no significant malformations post exposure, but yolk cysts were observed in groups exposed to PSNPs or AN, suggesting potential chorionic membrane penetration by PSNPs. At 96 hpf, all exposed groups showed enlarged yolk, black abdominal flocculence, lower melanin content, and oil sac development retardation, with the largest oil sacs in the AN group, followed by the AM and AgNPs groups. No significant differences in hatching rates were found among the exposed and control groups (Figure 2B). Cardiac assessments showed no abnormal heart rates in groups exposed solely to PSMPs or PSNPs (Figure 2C). However, zebrafish exposed to AgNPs alone had significantly lower heart rates ($p < 0.001$), an effect that was further exacerbated in groups with synergistic AN or AM exposure ($p < 0.01$, $p < 0.05$). The twitch frequency of embryos was significantly lower in the AN-treated larvae in comparison with the control (Figure 2D; $p < 0.001$), but not significantly different from the AgNPs-only group. AM treatment showed higher twitch frequencies compared with AN group ($p < 0.001$). Finally, all treated groups exhibited shorter body length in comparison with the control group (Figure 2E; $p < 0.001$, $p < 0.01$).

Measurements of Oxidative Stress in Zebrafish Induced by Combined Exposure

To elucidate the impact of combined exposure on oxidative stress in larval zebrafish, various oxidative stress markers were measured across different treatment groups. The accumulation of ROS was investigated first, and the results were shown in Figure 3A,B. In comparison with the control zebrafish, those exposed to PS M/NPs alone did not show a significant difference in ROS levels, but notably higher levels were observed in groups treated with AgNPs, AM, and AN ($p < 0.01$, $p < 0.05$, $p < 0.001$, respectively). In addition, a significantly higher MDA content was detected following 96-h exposure to these treatments (Figure 3C; $p < 0.001$), accompanied by notably lower GSH level in comparison with the control ($p < 0.05$, $p < 0.01$, $p < 0.001$, respectively).

Behavioral Assessment of Larval Zebrafish under Combined Exposure

To ascertain the potential neurotoxic effects of combined exposure to AgNPs and PS M/NPs in larval zebrafish, comprehensive behavioral analyses were performed using the Noldus Behavior Analysis Instrument. As depicted in Figure 4A, larvae in the control group exhibited normal movement patterns, whereas those exposed to AgNPs, AN, and AM showed significantly different behaviors, including lower movement pace and greater immobility. Quantitative analysis revealed a significantly shorter movement distance and lower velocity for these groups in comparison with the control (Figure 4B,C; $p < 0.01$, $p < 0.001$). An interesting finding was that larvae exposed to AM and AN displayed shorter movement distance, with a slightly higher but statistically insignificant swimming speed when compared with those exposed to AgNPs alone. The trajectory diagrams and heat map analysis (Figure 4A) suggested prolonged inactivity and uniform, circular motion patterns in the AN and AM groups, clarifying the paradox of higher speed levels yet shorter distance. Furthermore, in the turning angle test, significant differences in the movement angles of larval zebrafish in the AN and AM groups indicated heightened anxiety and fear states (Figure 4D), whereas the AgNPs, PSMPs, PSNPs, and control groups showed minor angle differences, underscoring the distinct neurotoxic impact of combined AgNPs and M/NPs exposure.

Under alternating light and dark conditions, the movement patterns of larval zebrafish in each experimental group exhibited periodic variations (Figure 4E). The control group exhibited normal responses to light–dark transitions, whereas PSNPs-exposed zebrafish exhibited significantly less active movement in darkness. For the AgNPs-containing exposure groups, the swimming distance in dark conditions followed the order: AN <AgNPs <AM.

In addition, an acoustic stimulation experiment was conducted to further assess the impact of combined exposure on behaviors of zebrafish larvae (Figure 4F). In comparison with the control and PS M/NPs groups, zebrafish exposed to AgNPs, AM, and AN showed significantly lower locomotor speeds, suggesting weaker and delayed responsive sensitivity to sound. During tapping stimulation, no significant differences in speed were observed between the AN and AM groups. However, both groups displayed an atypical pattern of speed variation, characterized by an initial decrease followed by an increase, along with delayed responsiveness.

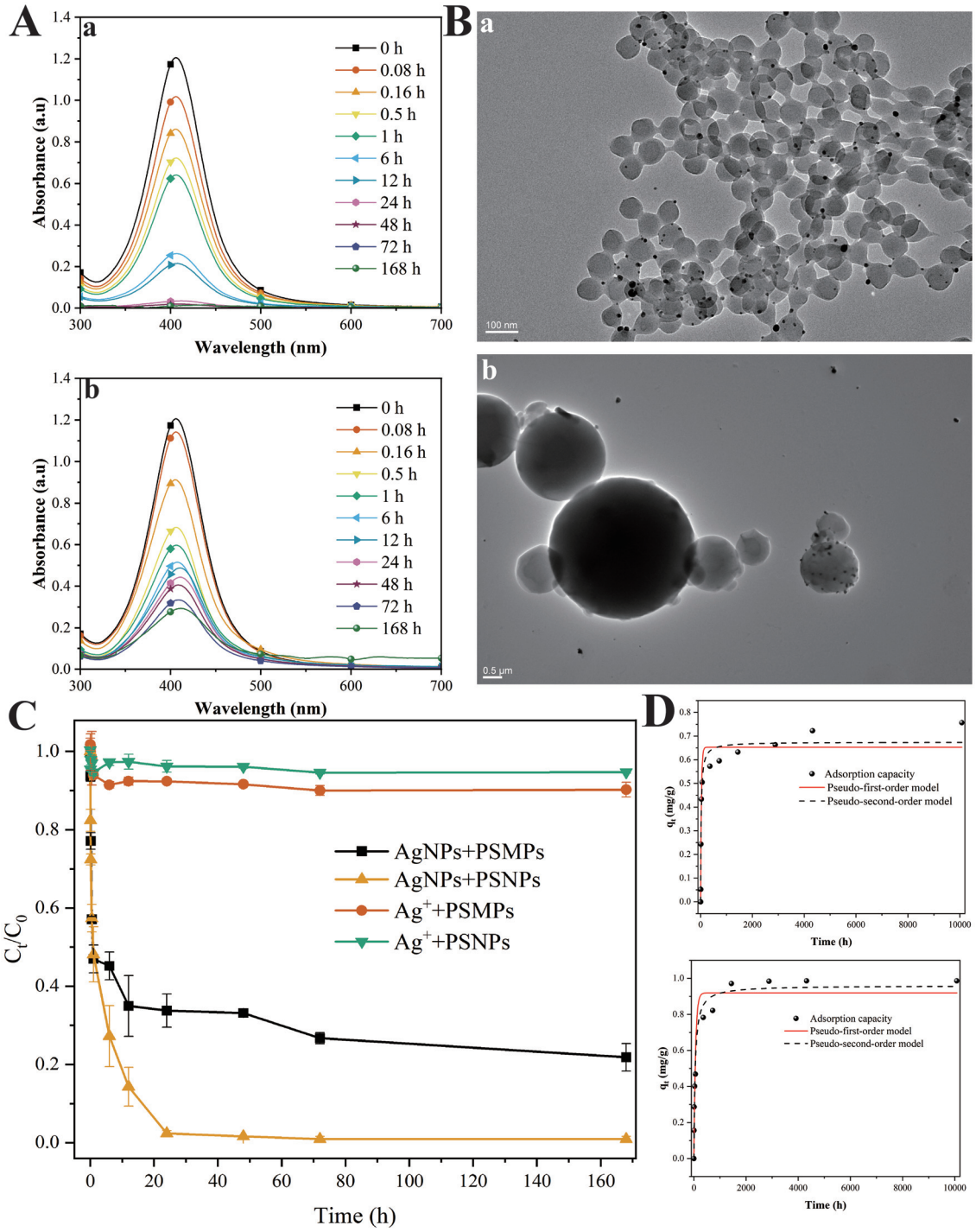

Figure 1. The interaction between PS M/NPs and AgNPs in ultrapure water. (A) UV absorption spectra of supernatants at different time periods after the adsorption of AgNPs onto PSNPs (a) or PSMPs (b). (B) TEM image of the complex of PSNPs-AgNPs (a) or PSMPs-AgNPs (b) after 168 h of adsorption. (C) Adsorption rate of AgNPs or Ag^+ by PS M/NPs at different time periods, C_0 and C_t denoting the initial and time-specific concentrations of AgNPs in the suspension (mg/L), respectively. (D) Pseudo primary kinetic model and pseudo secondary kinetic curves for the adsorption of AgNPs onto PSNPs (a) or PSMPs (b). The data are presented as the mean ± SD ($n = 3$). Data in Figure 1A–D are also presented in Excel Table S1. Note: AgNPs (silver nanoparticles, 5 nm): 10 mg/L; PS M/NPs (polystyrene micro/nanospheres, 5 μm/100 nm): 10 g/L; PSMPs, polystyrene microspheres; PSNPs, polystyrene nanospheres; SD, standard deviation; TEM, transmission electron microscope; UV, ultraviolet.

To explore the link between AgNPs-induced motor behavior abnormalities and motor function/neural circuitry in zebrafish, larvae from various treatment groups at 96 hpf were subjected to tactile stimuli using a straw, with locomotor and escape responses recorded via video tracking (Figure 4G). Larvae in the control group exhibited high-frequency muscle contractions, allowing them to rapidly escape from the stimulus within 0.1 s. Their response involved rapid, alternating trunk contractions, indicating efficient neuromuscular coordination. In contrast, larvae exposed to PS M/NPs alone showed no significant changes in tactile response in comparison with the control. However, the larval zebrafish in the AgNPs-containing exposure groups exhibited slower responses

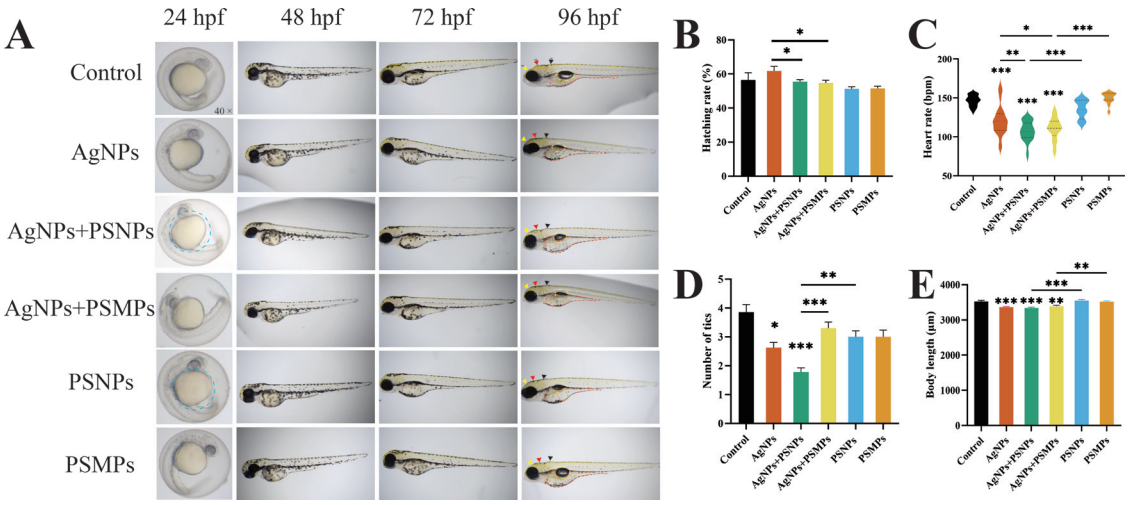

Figure 2. Developmental outcomes in larval zebrafish exposed to control, AgNPs, PSNPs, PSMPs, or a combination of AgNPs with either PSNPs or PSMPs. (A) Morphological observations of zebrafish larvae (96 hpf) development; blue dotted line: abnormal yolk development; yellow dashed line: abnormal swim bladder development; red dashed line: abnormal yolk development; yellow, red and blue arrows represent the forebrain, mesencephalon, and hindbrain, respectively. (B) The hatching rate (%) of zebrafish at 48 hpf. (C) The heart rate of zebrafish at 48 hpf. (D) The number of twitching (beats per minute) in zebrafish at 48 hpf. (E) The body length of zebrafish at 96 hpf. The data are presented as the mean ± SD ($n = 3$ pools of 30 individuals per pool). Statistical comparisons were performed using ANOVA followed by Tukey's method. Data in Figure 2B–E are also presented in Excel Table S2. Unless otherwise stated, the concentrations for single or combined exposures are as follows: AgNPs: 10 μg/L; PSNPs: 200 μg/L; PSMPs: 200 μg/L. All experimental subjects were AB wild-type zebrafish. Note: AgNPs, silver nanoparticles; ANOVA, analysis of variance; hpf, hours post fertilization; PSNPs, polystyrene nanospheres; PSMPs, polystyrene microspheres; SD, standard deviation. Significance levels: $^{*}p < 0.05$, $^{**}p < 0.01$, and $^{***}p < 0.001$.

and shorter movement distances than control group, following the order: AN < AM < AgNPs.

The Effects on the Development of the Nervous System of Larval Zebrafish under Combined Exposure

In light of the observed abnormal motor behaviors in zebrafish due to combined exposure, a detailed investigation was conducted to assess the impact on neurodevelopment. Given the pivotal role of *elavl3* in the early neurodevelopment of zebrafish and its status as a key marker gene for nervous system development, 72-hpf Tg (*elavl3*:EGFP) transgenic zebrafish were used to elucidate the effects of combined exposure on the development of the zebrafish nervous system. As shown in Figure 5A, the group treated with AgNPs exhibited a significant reduction in *elavl3* expression, diminished neuron count in the brain, and a less distinct separation between the diencephalon and hindbrain in comparison with the control group. Notably, the AN group showed apparent neuron axon shortening and hypoplasia in the optic tectum and cerebellum. In the AM group, underdevelopment of the cerebellum and indistinct cerebellar boundaries were observed. Furthermore, the expression of *elavl3* in the head region of larval zebrafish was quantitatively analyzed for each treatment group (Figure 5B). When compared with the control group, those exposed to PS M/NPs alone did not have significantly different numbers of neonatal neurons. However, a notable difference in neonatal neuron numbers was observed in treatments involving AgNPs, AN, and AM exposure ($p < 0.001$, $p < 0.001$, $p < 0.05$), respectively.

The activity of AChE, which plays a critical role in sensory and neuromuscular functions,[46] was further evaluated following combined exposure. As shown in Figure 5C, a marked inhibition of AChE activity was observed in AgNPs group in comparison with the control group ($p < 0.05$), with AN further intensifying this effect ($p < 0.01$). However, no significant differences in AChE activity were observed in the AM group.

Subsequently, this study used Tg (*kdrl*:mCherry) zebrafish, exposed from 6 to 120 hpf, to examine the effects of coexposure to AgNPs and PS M/NPs on vascular development (Figure 5D). In comparison with the control group, AgNPs exposure led to thinner and more disorganized vasculature in the eyes of larval zebrafish. Zebrafish exposed to PS M/NPs alone demonstrated mild vascular dysplasia. More pronounced effects were observed in the AM and AN groups, characterized by significant intracranial vascular ablation and disordered arrangement, with these effects being most pronounced in the AN group. To quantify these differences, a vascular network analysis was conducted using Angio Tool software.[47] This analysis revealed that exposure to AM/AN resulted in shorter vessel length in larval zebrafish in comparison with the control ($p < 0.05$), with the AN group also showing smaller vascular area and greater porosity (Figure 5F–H; $p < 0.01$, $p < 0.05$). In comparison with the AgNPs group, both the AN and AM groups exhibited shorter vessel lengths and smaller vascular areas, with the differences being more pronounced in the AN group. However, these differences were not statistically significant.

Moreover, this study aimed to investigate whether the lower levels of neural marker expression and abnormal vascular development, associated with combined exposure, are correlated with apoptosis. AO staining was employed to examine apoptotic events in the heads of larval zebrafish (Figure 5E,I). It was observed that pronounced apoptotic signals occurred in the AgNPs-treated group in comparison with control ($p < 0.001$), especially in the brain and yolk region. The AN group showed significant apoptosis in various organs, including the heart, brain, and liver ($p < 0.001$), whereas the AM group exhibited apoptosis in the heart, brain, and digestive tract ($p < 0.001$). Further quantitative analysis revealed that AN treatment notably exhibited greater apoptosis in the brain in comparison with AgNPs ($p < 0.01$), suggesting an exacerbation of CNS damage.

The Effects on the Immune System in Larval Zebrafish under Combined Exposure

In the innate immune system, macrophages play a vital role in early vertebrate development and immune response. Neutral red, an alkaline phenazine dye, effectively stains lysosomes red and can be used to mark macrophages within zebrafish. As shown in

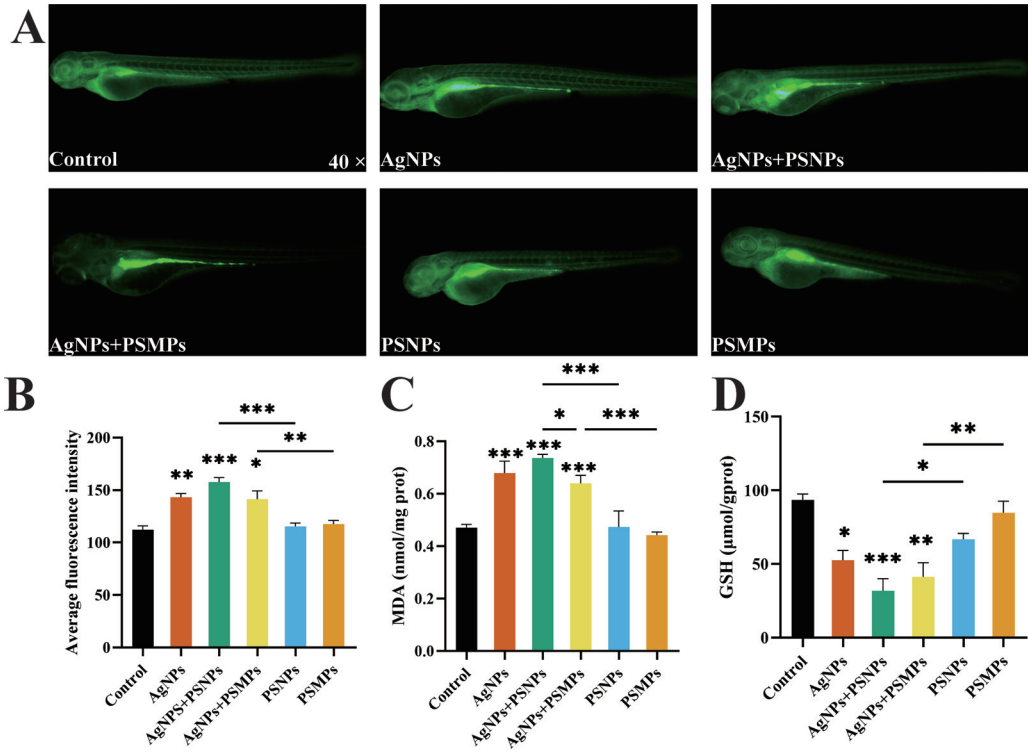

Figure 3. Analysis of oxidative stress in larval zebrafish exposed to control, AgNPs, PSNPs, PSMPs, or a combination of AgNPs with either PSNPs or PSMPs. (A) Accumulation of ROS (green) in zebrafish larvae at 72 hpf. (B) The quantitative analysis of ROS accumulation. (C, D), Differences in the level of MDA (C: $n = 3$ pools of 50 individuals per pool) and GSH (D: $n = 3$ pools of 50 individuals per pool) in zebrafish larvae. The data are presented as the mean ± SD (unless otherwise stated; $n = 3$ pools of 30 individuals per pool). Data in Figure 3B–D are also presented in Excel Table S3. Statistical comparisons were performed using ANOVA followed by Tukey's method. Unless otherwise stated, the concentrations for single or combined exposures are as follows: AgNPs: 10 μg/L; PSNPs: 200 μg/L; PSMPs: 200 μg/L. All experimental subjects were AB wild-type zebrafish. Note: AgNPs, silver nanoparticles; ANOVA, analysis of variance; GSH, glutathione; hpf, hours post fertilization; MDA, malondialdehyde; PSMPs, polystyrene microspheres; PSNPs, polystyrene nanospheres; ROS, reactive oxygen species; SD, standard deviation. Significance levels: $^{*}p < 0.05$, $^{**}p < 0.01$, and $^{***}p < 0.001$.

Figure 6A,B, larval zebrafish in the exposed group displayed a significantly higher number of macrophages in the head region in comparison with the control group ($p < 0.01$, $p < 0.001$). Specifically, the AN group exhibited a significantly higher number of macrophages than the AgNPs group ($p < 0.05$), whereas the AM group showed no marked difference.

To further elucidate the impact of combined exposure on the innate immune response in zebrafish larvae, we employed a Tg (*coro1a*: EGFP) transgenic zebrafish line. This strain effectively labeled both macrophages and neutrophils, enabling the tracking of innate immune cells in zebrafish. As depicted in Figure 6C,D, we conducted a quantitative analysis of the fluorescence intensity of these innate immune cells, specifically in the region superior to the zebrafish abdomen. Notably, our findings revealed a significantly higher level in the fluorescence intensity of innate immune cells within the AN group, in contrast to the control and PSNPs groups ($p < 0.05$, $p < 0.01$).

The Exploration of Potential Mechanisms Underlying Neurotoxicity Induced by Combined Exposure

To elucidate the molecular dynamics underlying the aberrant development of the nervous system upon combined exposure, qPCR was employed to assess the differential expression of key genes involved in neurovascular system development across different exposure groups. These genes included neurodevelopmental genes (*pax6a*, *elavl3*, *egr2b*, *ptafr*, *gabbr1a*, and *gabbr1b*) and vascular development genes (*kdrl* and *fli1a*) (Figure 7). Our findings indicated a marked down-regulation of *elval3*, *pax6a*, and *egr2b* in the AgNPs-containing treatment group in comparison with control group ($p < 0.05$, $p < 0.01$, $p < 0.001$). The AN group exhibited the lowest expression levels, differing significantly from both AgNPs ($p < 0.05$, $p < 0.01$) and AM ($p < 0.05$, $p < 0.001$) groups. *pax6a* expression was notably higher in the AM group in comparison with AgNPs ($p < 0.05$), whereas *elval3* and *egr2b* did not show significant differences in comparison with the AgNPs group. This molecular evidence suggested that AN significantly intensified the neurotoxic impacts of AgNPs, whereas AM distinctly altered their neurotoxic effects. In addition, combined exposure of AM/AN led to a significantly lower levels in *fli1a* and *kdrl* expression ($p < 0.01$, $p < 0.001$), aligning with previous vascular analysis. Exposure to AN significantly up-regulated *ptafr* expression ($p < 0.05$), with no notable difference between AM and AgNPs. The differential expression patterns of *gabbr1a* and *gabbr1b* in response to combined exposure could be ascribed to distinct mechanisms, potentially related to the variation in particle sizes of PS M/NPs.

To further investigate the potential mechanisms underlying neurodevelopmental and neuroimmune damage in zebrafish induced by combined exposures, we quantitatively assessed apoptosis- and immune-related gene expression. As depicted in Figure 7, the expressions of apoptosis-related genes (*caspase3* and *caspase9*) in the AgNPs-containing treatment groups were significantly higher than those in the control group ($p < 0.05$, $p < 0.01$, $p < 0.001$), whereas no significant changes differences were observed in the PS M/NPs group. In comparison with the AgNPs group, the AN group demonstrated a significantly higher levels in the expression of these genes ($p < 0.05$), whereas in the AM group, there was a slight down-regulation of *caspase3* and a slight up-regulation of *caspase9*. The results indicated that AgNPs, AM, and AN exposure led to apoptosis in zebrafish

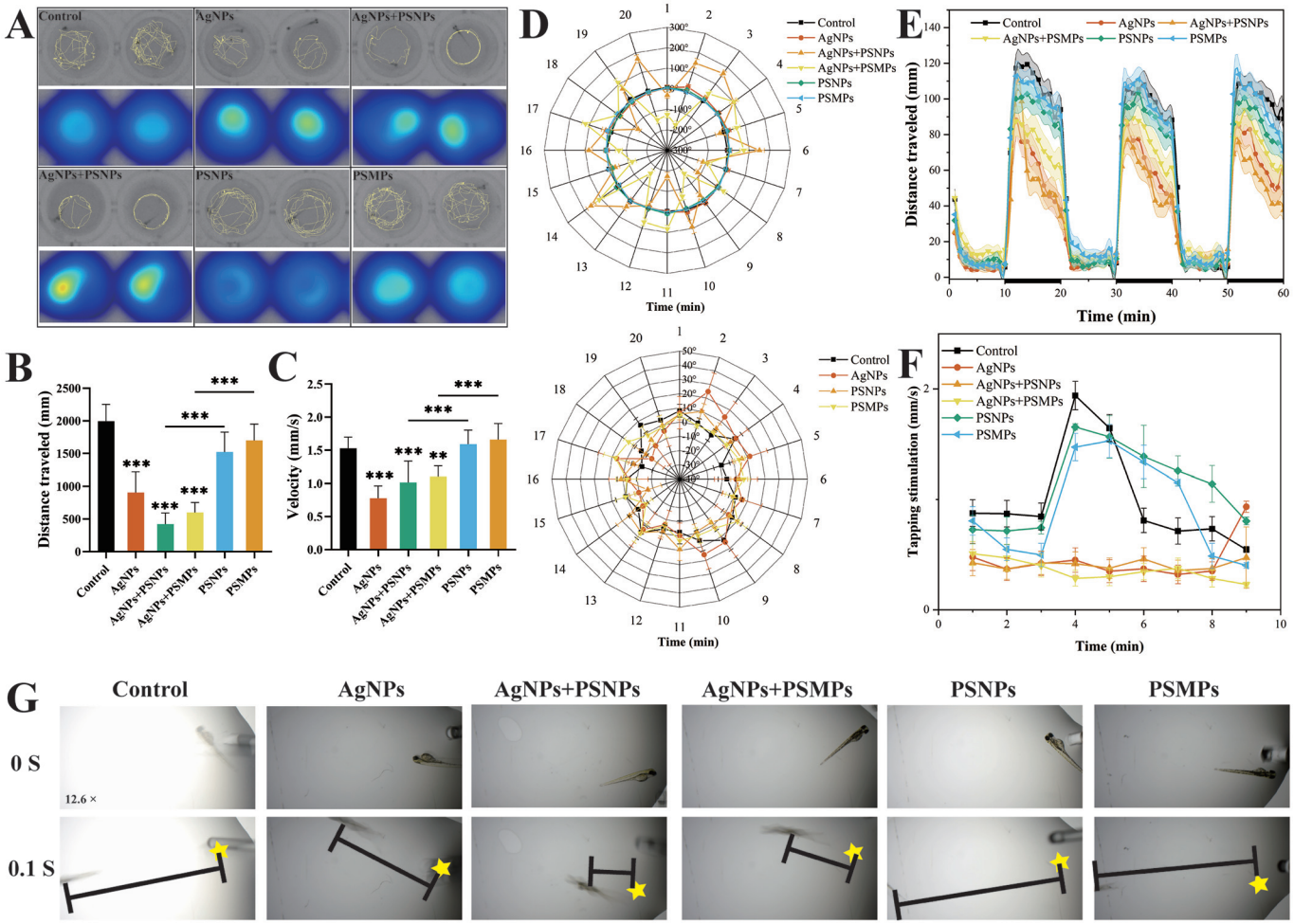

Figure 4. Behavioral outcomes in larval zebrafish exposed to control, AgNPs, PSNPs, PSMPs, or a combination of AgNPs with either PSNPs or PSMPs. (A) The trajectory and heat map of the autonomous motion in larval zebrafish (120 hpf); The quantitative analysis of swimming distance (B) and average speed (C) of larval zebrafish; (D) Turning angle radar chart, with the lower part of the chart showing an enlarged view of the −40° to 50° segment. (E) The swimming distance of larval zebrafish (120 hpf) when experiencing a 60-min dark-to-light photoperiod transition. (F) Velocity diagram of acoustic stimulation movement of larval zebrafish. (G) Touch response of 96-hpf zebrafish larvae; The black line: the distance of movement. The yellow pentagram: the initial position of the zebrafish larvae. Behavioral analysis by recording a 1-s motion trajectory video, segmented into 0.1-s image frames. The data are presented as the mean ± SD (unless otherwise stated, $n = 3$ pools of 30 individuals per pool). Data in Figure 4B–F are also presented in Excel Table S4. Statistical comparisons were performed using ANOVA followed by Tukey's method. Unless otherwise stated, the concentrations for single or combined exposures are as follows: AgNPs: 10 μg/L; PSNPs: 200 μg/L; PSMPs: 200 μg/L. All experimental subjects were AB wild-type zebrafish. Note: AgNPs: silver nanoparticles; ANOVA, analysis of variance; hpf, hours post fertilization; PSMPs, polystyrene microspheres; PSNPs, polystyrene nanospheres; SD, standard deviation. Significance levels: $^{*}p < 0.05$, $^{**}p < 0.01$, and $^{***}p < 0.001$.

larvae by up-regulating *caspase3* and *caspase9*. Concurrently, the extent of apoptosis was most pronounced in the AN group. In addition, some immune-related genes (*tnfα*, *il10*, and *il10ra*) were detected in larval zebrafish under different treatments from 6 hpf to 120 hpf. As shown in Figure 7, the expressions of *tnfα* in AgNPs, AN, and AM groups were prominently higher than those in the control group ($p < 0.001$, $p < 0.001$, $p < 0.001$). In comparison with AgNPs and AM groups, *tnfα* was notably up-regulated in the AN group ($p < 0.001$, $p < 0.01$). This finding suggested that AN activated the most inflammatory cytokines among all the treatments. In the AgNPs-containing treatment groups, the expressions of *il10* were significantly higher than those in control group ($p < 0.01$, $p < 0.001$), with expression levels following the order: AgNPs > AN > AM. When compared to the control group, the AgNPs group exhibited significantly higher expression level of *il10ra* ($p < 0.01$), whereas the expression levels of *il10ra* in the AN and AM groups were slightly lower ($p < 0.05$).

Furthermore, the types of combined effects of AgNPs and PS MPs/NPs on the above neuroinflammation were evaluated by Equation 5, with the results summarized in Table S3. For vascular, behavioral, oxidative stress, and immune-related end points, the majority of the combined effects between AgNPs and PS MPs/NPs were synergistic (ratio <1, $p < 0.05$). However, for a few end points, such as ROS, MDA, and macrophages, the combined effects of AM were antagonistic (ratio <1, $p < 0.05$). In contrast, for inflammation-, vascular-, and neuron-related genes, the combined effects of AgNPs and PS MPs/NPs were additive ($p > 0.05$). Overall, most of the ratios in Table S3 exceed 1, with several showing p-values <0.05. Furthermore, the majority of ratio values in the AN group were higher than those in the AM group. These results indicated that coexposure to AgNPs and PS MPs/NPs led to a significant potentiation effect, with the enhancement effect being more pronounced for AN.

Evaluation of the Contribution of Dissolved Silver Ions in AgNPs-Induced Neurotoxicity

Given that AgNPs can dissolve in water and release Ag^{+}, we further explored the contribution of silver ions to the neurotoxicity

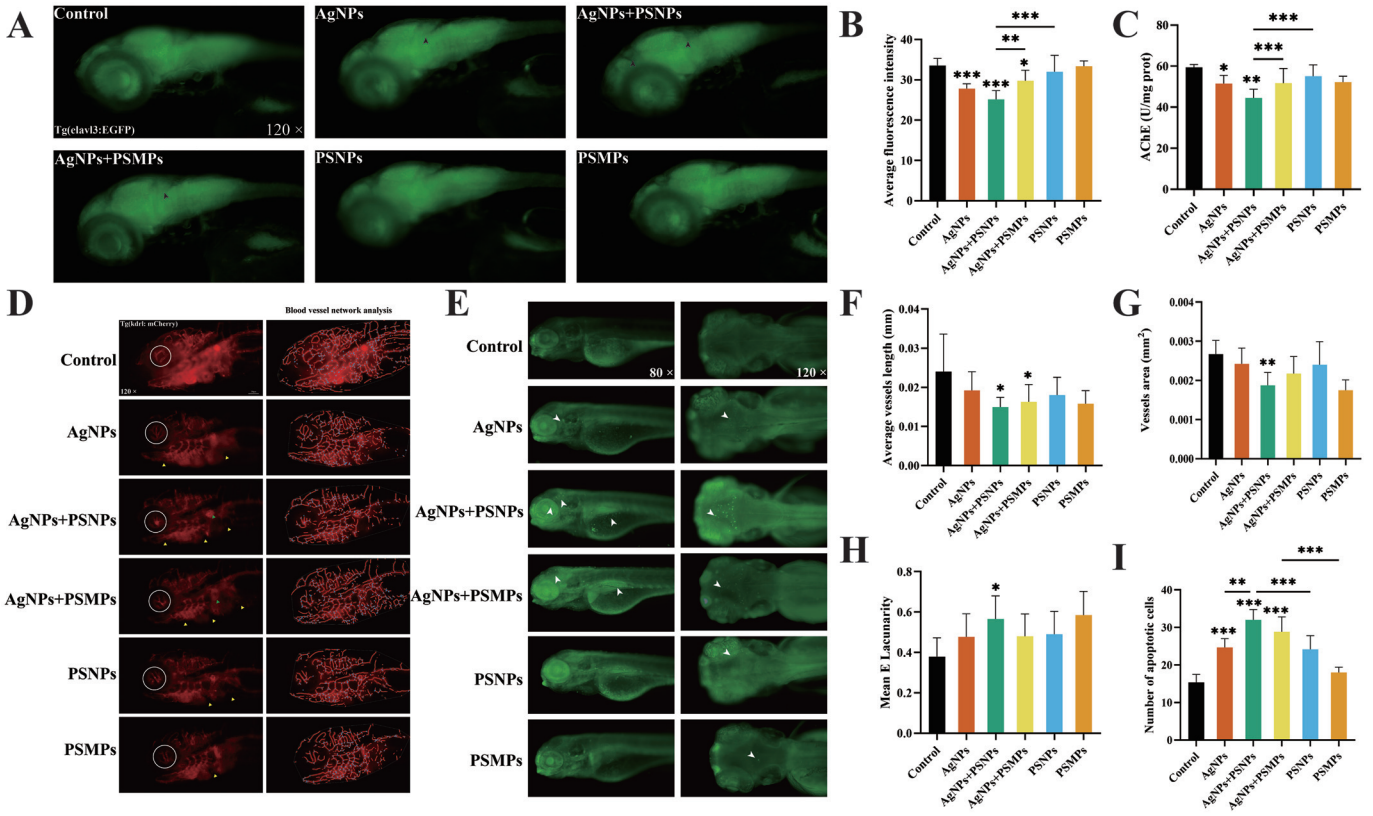

Figure 5. Observations on neural and vascular development in larval zebrafish exposed to control, AgNPs, PSNPs, PSMPs, or a combination of AgNPs with either PSNPs or PSMPs. (A) Differences in *elavl3* expression observed in Tg(*elavl3*:EGFP) transgenic zebrafish larvae at 96 hpf under combined exposure. (B) The quantification of fluorescence intensity regarding *elavl3* expression. (C) Differences in AChE levels in zebrafish larvae (96 hpf). (D) Vascular phenotype observation in Tg(*kdrl*:mCherry) transgenic zebrafish larvae at 96 hpf. Right column: the vascular network map analysis. (E) The observation of cell apoptosis in 96 hpf larval zebrafish. (F–H) The quantification of vascular network analysis; mean vessel length (F), vessel area (G), and porosity (H). (I) The quantification of the number of apoptotic cells. The data are presented as the mean ± SD (unless otherwise stated, $n = 3$ pools of 30 individuals per pool). Statistical comparisons were performed using ANOVA followed by Tukey's method. Data in Figure 5B–I are also presented in Excel Table S5. Unless otherwise stated, the concentrations for single or combined exposures are as follows: AgNPs: 10 μg/L; PSNPs: 200 μg/L; PSMPs: 200 μg/L. The experimental subjects: (A–C) Tg(*elavl3*:EGFP) transgenic zebrafish; (D,F–H) Tg(*kdrl*:mCherry) transgenic zebrafish; (E and I) AB wild-type zebrafish. Note: AChE, acetylcholinesterase; AgNPs, silver nanoparticles; ANOVA, analysis of variance; EGFP, enhanced green fluorescent protein; *elavl3*, embryonic lethal, abnormal vision, *Drosophila*-like 3; hpf, hours post fertilization; *kdrl*, kinase insert domain receptor-like; mCherry, monomeric Cherry; PSMPs, polystyrene microspheres; PSNPs, polystyrene nanospheres; SD, standard deviation. Significance levels: $^{*}p < 0.05$, $^{**}p < 0.01$, and $^{***}p < 0.001$.

induced by AgNPs. As shown in Figure 8A, the dissolution rate of AgNPs was rapid during the initial 72 h, gradually leveling off and reaching a final concentration of 4 μg/L at 168 h. After the combination with PS M/NPs, the dissolution rate of AgNPs was significantly lower than that of AgNPs alone, with Ag^{+} concentrations at 168 h were 2.34 and 2.69 μg/L, respectively. To investigate the neurotoxic effects of AgNPs on zebrafish and determine the contributions from the AgNPs themselves vs. dissolved silver ions, AgNPs (10 μg/L) and $AgNO_3$ (2.2 μg/L) were selected to expose larval zebrafish. The exposure concentration of $AgNO_3$ was determined based on the concentration of dissolved silver ions released from AgNPs (10 μg/L) after 24 h, as the exposure medium for the larvae was replaced every 24 h. First, the Ag contents in larval zebrafish after 96 h of exposure to AgNPs and $AgNO_3$ were measured to assess Ag accumulation *in vivo* (Figure 8B). The results indicated that the accumulation of AgNPs in zebrafish larvae was significantly higher than that of the $AgNO_3$ group ($p < 0.001$), suggesting that AgNPs themselves can be taken up by the larvae in particulate form in addition to the released silver ions. In addition, the contents of Ag in the AN and AM groups were prominently higher than that in AgNPs group ($p < 0.001$), which indicated that the combined exposure induced more Ag accumulation in larval zebrafish than AgNPs alone. As shown in Figure 8C,D, it was evident that the accumulation of ROS induced by AgNPs was significantly greater than that induced by $AgNO_3$ ($p < 0.01$). Further investigations using the transgenic strain Tg(*elavl3*:EGFP) revealed the impact of AgNPs and $AgNO_3$ exposure on neuronal development in zebrafish (Figure 8C). Fluorescent quantitative analysis showed that the fluorescence intensity of neurons in the brains of larvae exposed to AgNPs was slightly lower than that in the $AgNO_3$ group (Figure 8E), suggesting that AgNPs exerted a stronger inhibitory effect on neuronal development. In addition, behavioral experiments demonstrated that zebrafish larvae exposed to AgNPs exhibited significantly lower swimming speed ($p < 0.01$) and shorter distance ($p < 0.001$) in comparison with the $AgNO_3$ group (Figure 8F,H,I), indicating poorer locomotor activity. The light–dark cycle experiments also revealed that the movement distance of larvae in the dark was significantly longer in the AgNPs exposure group than that in the $AgNO_3$ group (Figure 8G), suggesting a more pronounced anxiety response in dark conditions. Based on the summary from Table S4, the contribution of silver ions to various toxicity indicators was approximately within the range of 33%–58%, suggesting that the neurotoxicity induced by AgNPs resulted from both the nanoparticles themselves and the dissolved silver ions.

To assess whether PS M/NPs can be taken up by zebrafish, thereby influencing AgNPs accumulation within the organism,

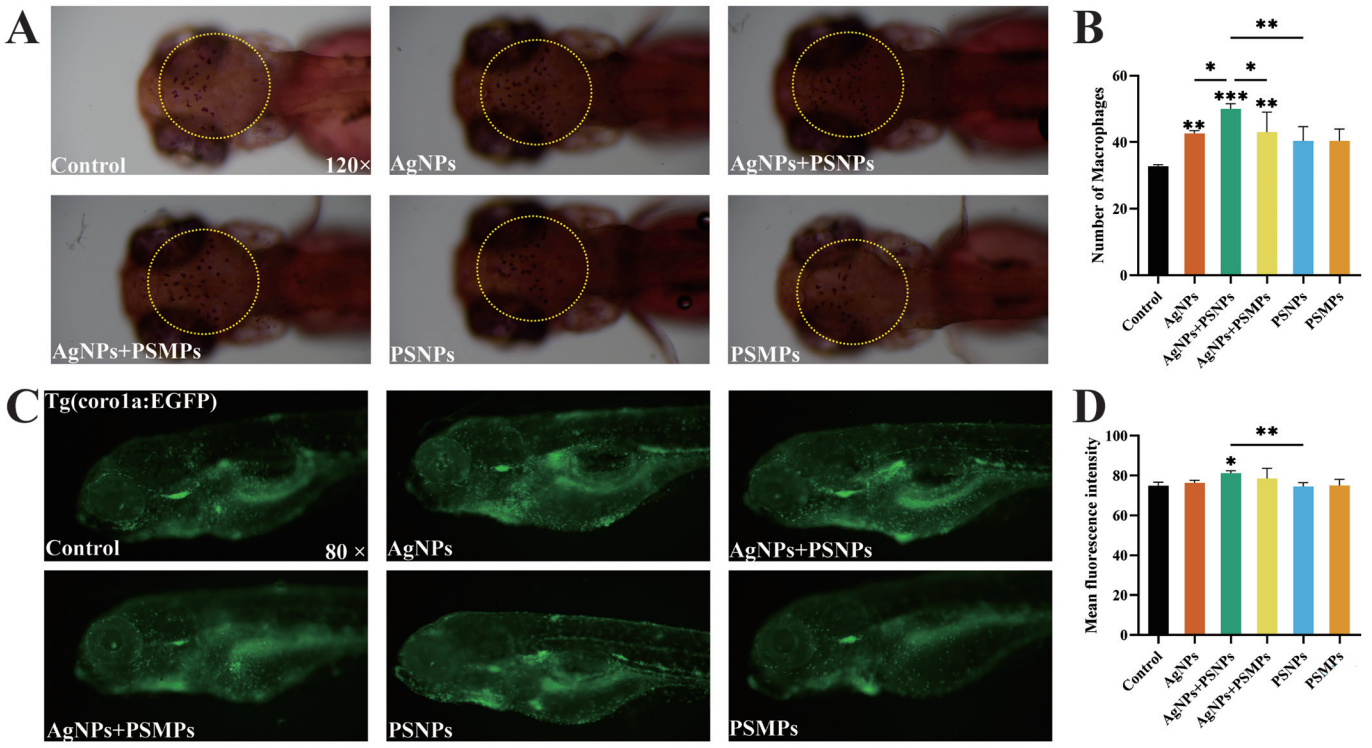

Figure 6. Effects on immune cells in larval zebrafish after exposure to control, AgNPs, PSNPs, PSMPs, or a combination of AgNPs with either PSNPs or PSMPs. (A) Differences in the macrophages of the head region in zebrafish larvae at 96 hpf. (B) The quantification of macrophages in the head of zebrafish larvae. (C) The number of innate immune cells observed in Tg(*coro1a*: EGFP) transgenic zebrafish larvae at 72 hpf. (D) The quantification of innate immune cells. The data are presented as the mean ± SD (unless otherwise stated, $n = 3$ pools of 30 individuals per pool). Data in Figure 6B,D are also presented in Excel Table S6. Statistical comparisons were performed using ANOVA followed by Tukey's method. Unless otherwise stated, the concentrations for single or combined exposures are as follows: AgNPs: 10 μg/L; PSNPs: 200 μg/L; PSMPs: 200 μg/L. The experimental subjects: AB wild-type zebrafish (A and B); Tg(*coro1a*:EGFP) transgenic zebrafish (C and D). Note: AgNPs, silver nanoparticles; ANOVA, analysis of variance; *coro1a*, coronin 1A; EGFP, enhanced green fluorescent protein; hpf, hours post fertilization; PSMPs, polystyrene microspheres; PSNPs, polystyrene nanospheres; SD, standard deviation. Significance levels: $^{*}p < 0.05$, $^{**}p < 0.01$, and $^{***}p < 0.001$.

zebrafish embryos at 6 hpf were exposed to Cy5-labeled PS M/NPs at a concentration of 1 mg/L with the same fluorescence intensity (Figure 8J). The distribution of PS M/NPs within embryos or larvae was observed across different developmental stages. At 24 hpf, red fluorescence from the PSMPs group was predominantly located around the chorion, whereas red fluorescence from the PSNPs group was concentrated within the embryo, indicating that most PSNPs penetrated the chorion and were taken up by the embryo, whereas PSMPs accumulated around the chorion without entering. At 48–72 hpf, larvae were fully hatched from the chorion, and organ formation progressed at 96 hpf. At 72 hpf, red fluorescence in both the PSMPs and PSNPs groups was primarily concentrated in the yolk sac tissue. By 120 hpf, with fully developed intestines and the onset of feeding, zebrafish larvae in the PSMPs and PSNPs groups displayed high-intensity fluorescence in the intestinal and pancreatic regions, with minor accumulation observed in the eyes. Further quantitative analysis shown in Figure 8K showed that with extended exposure time, zebrafish presented increased uptake of PS M/NPs, with a significantly higher uptake efficiency for PSNPs in comparison with PSMPs ($p < 0.01$).

Evaluation of the Effects of Curcumin on Neurotoxicity Induced by Combined Exposure

To further investigate the mechanisms of neurotoxicity induced by combined exposure, the natural antioxidant curcumin (200 μg/L) was introduced as a therapeutic agent to assess its effects on neurotoxicity under combined exposure. As shown in Figure 9A,B, curcumin significantly ameliorated the effects of AgNPs alone, with improved diencephalon development, clearer boundaries, and a significantly stronger fluorescence intensity in comparison with AgNPs exposure ($p < 0.01$). However, its remedial effects on the AN group were less apparent, characterized by incomplete diencephalon development, blurred boundaries, and slightly weaker average fluorescence intensity. Curcumin also had a certain rescuing effect on the AM treatment group, with clearer diencephalon boundaries and a significantly stronger fluorescence intensity ($p < 0.05$). Using Tg(*kdrl*:mCherry) transgenic zebrafish, the vascular recuperative effects of curcumin were assessed. As illustrated in Figure 9A,C,D, curcumin was observed to partially restore the cerebral vasculature, evidenced by lower vascular porosity and larger average vessel area following AgNPs exposure. However, its impact on cranial vessels in the AN and AM groups was comparatively modest. Behavioral analysis further indicated that the larval zebrafish in the AgNPs + curcumin group exhibited higher autonomous movement speed and longer distance than those in the group exposed to AgNPs alone (Figure 9E,F; $p < 0.05$, $p < 0.01$). In addition, in the light–dark rhythm experiments, the addition of curcumin resulted in longer swimming distances for AgNPs-exposed zebrafish larvae under dark conditions and exhibited a partial restorative effect for larvae in the AM/AN exposure groups (Figure 9G).

The values of various experimental indicators for different groups, normalized to the control group, were summarized in the heat map displayed in Figure S3A. It can be observed that for most neuro- and immune-related indicators, the toxicity of the AgNPs + PSMPs group was slightly stronger than that of the AgNPs group, whereas the AgNPs + PSNPs group exhibited the

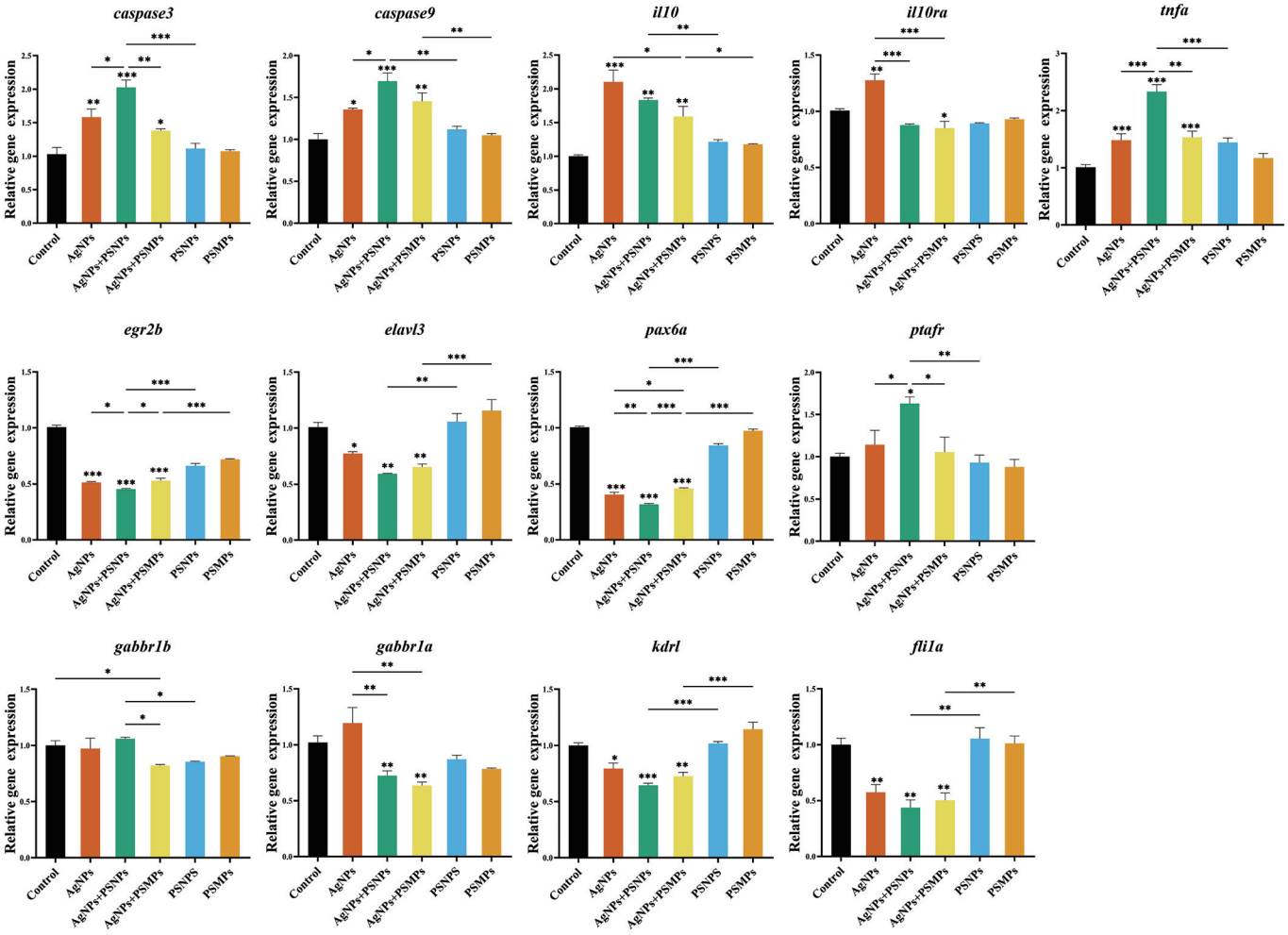

Figure 7. The expression of genes related to apoptosis, immunity, neurodevelopment, and vascular development in larval zebrafish exposed to control, AgNPs, PSNPs, PSMPs, or a combination of AgNPs with either PSNPs or PSMPs. The data are presented as the mean ± SD (unless otherwise stated, $n = 3$ pools of 50 individuals per pool). Statistical comparisons were performed using ANOVA followed by Tukey's method. Data in Figure 7 are also presented in Excel Table S7. Unless otherwise stated, the concentrations for single or combined exposures are as follows: AgNPs: 10 μg/L; PSNPs: 200 μg/L; PSMPs: 200 μg/L. All experimental subjects were AB wild-type zebrafish. Note: AgNPs, silver nanoparticles; ANOVA, analysis of variance; *caspase3*, cysteine-aspartic protease 3; *caspase9*, cysteine-aspartic protease 9; *egr2b*, early growth response 2b; *elavl3*, embryonic lethal, abnormal vision, *Drosophila*-like 3; *fil1a*, filamin A; *gabbr1a*, gamma-aminobutyric acid B receptor 1A; *gabbr1b*,x gamma-aminobutyric acid B receptor 1b; *il10*, interleukin-10; *il10rα*, interleukin-10 receptor α; *kdrl*, kinase insert domain receptor-like; *pax6a*, paired box gene 6A; PSMPs, polystyrene microspheres; PSNPs, polystyrene nanospheres; *ptafr*, prostaglandin F2 α receptor; SD, standard deviation; *tnfa*, tumor necrosis factor-α. Significance levels: $^{*}p < 0.05$, $^{**}p < 0.01$, and $^{***}p < 0.001$.

highest toxicity. The values of the rescue experimental indicators for different groups after the addition of curcumin and normalized to the control group were presented in Figure S3B. The incorporation of curcumin demonstrated a significant rescue effect in the AgNPs group, whereas its efficacy was relatively weak in the combined exposure group.

Comparative Neurotoxic Effects of Different MPs in Combined Exposure with AgNPs

Although our study used PS M/NPs as representatives, to assess the broader applicability of our findings to a wider range of microplastics, we incorporated MPs with different charges, specifically PLA MPs and PA MPs, along with PSMPs of mixed particle sizes, and subjected them to combined exposure with AgNPs to compare their neurotoxic effects. As shown in Figure S4A,D, the ROS accumulation in the PLA/PA + AgNPs groups was significantly lower than that observed in the AgNPs group ($p < 0.001$), whereas the Mix + AgNPs group exhibited significantly greater ROS accumulation in comparison with the AgNPs group ($p < 0.001$), consistent with the trend observed in the PSNPs + AgNPs group. Furthermore, zebrafish in the PLA/PA + AgNPs groups displayed significantly lower swimming speed and shorter distance in comparison with those in the AgNPs group ($p < 0.001$; Figure S4B,E,F). In the light–dark rhythm experiment, zebrafish in the PLA/PA + AgNPs groups traveled a greater distance in the dark in comparison with the AgNPs group, whereas the Mix + AgNPs group exhibited the opposite trend (Figure S4C).

Discussion

Recent research has highlighted that microplastics act as vectors for contaminant transport, thereby modifying the bioavailability of toxins and reshaping environmental risk profiles.[48,49] Consequently, the environmental impact of microplastics has become an increasing concern. Among prevalent nanomaterials, AgNPs share a similar environmental fate as microplastics, a concern exacerbated by the recent coronavirus pandemic. Our study centered on the interplay between microplastics and AgNPs, particularly focusing on the resultant neurotoxic effects from their combined exposure.

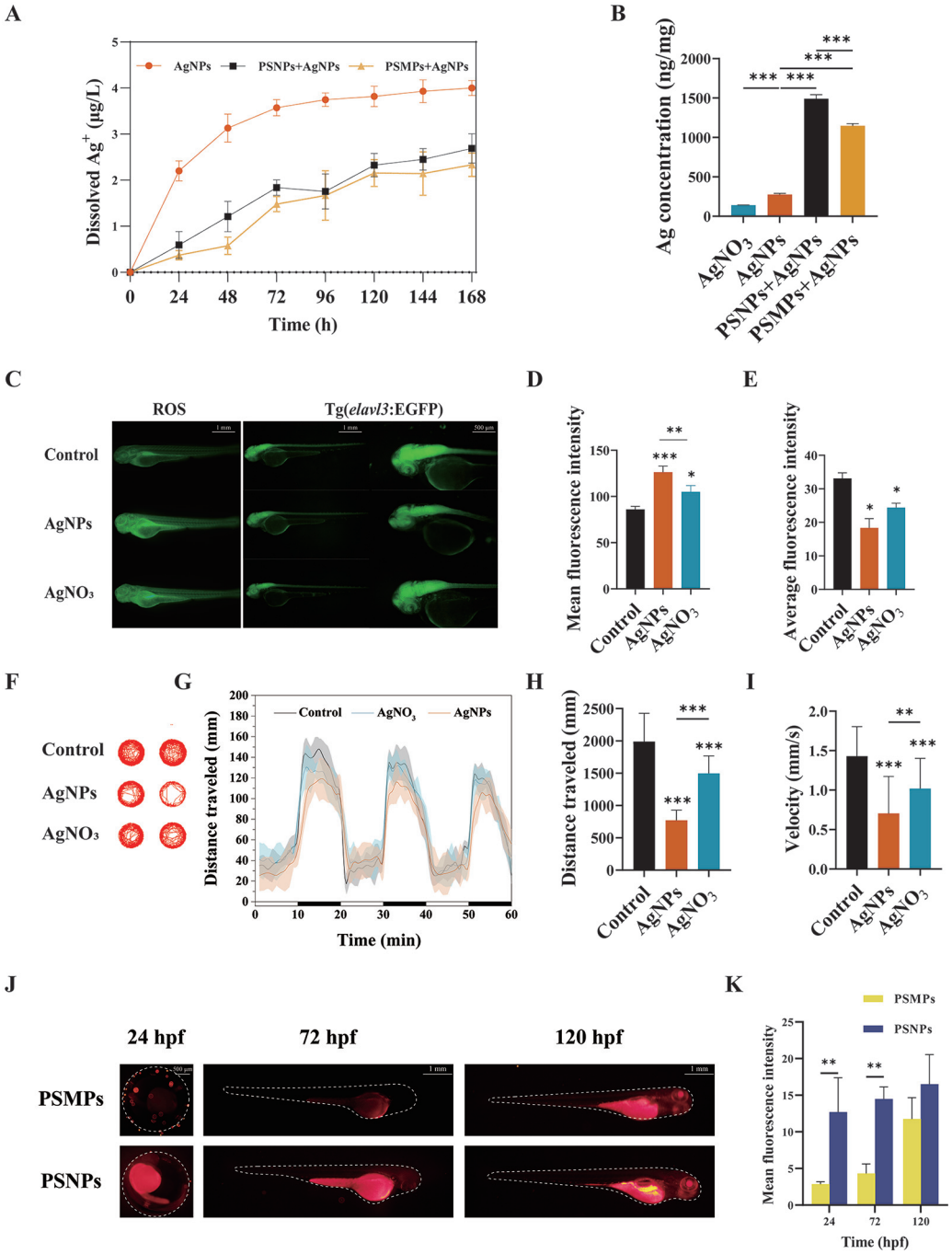

Figure 8. Comparative analysis of the effects on the nervous system in zebrafish larvae exposed to AgNPs and $AgNO_3$. (A) The dissolution rate of AgNPs before and after combination with PS M/NPs in water over 7 days. (B) Silver concentration in zebrafish larvae (96 hpf) after exposure to $AgNO_3$, AgNPs and PS M/NPs + AgNPs. (C) ROS staining of 72-hpf larvae and the phenotypic observation of the brain in Tg (*elavl3*: EGFP) larvae. (D) Quantitative analysis of ROS staining. (E) Average fluorescence intensity regarding *elavl3* expression in the brain. (F) Autonomous motion trajectory of 120-hpf larvae for 20 min. (G) Locomotor activity of 120 hpf larvae in response to alternating light and dark conditions. (H,I) The quantitative analysis in autonomous locomotion assays; Movement distance (H), and Velocity (I). (J,K) The uptake and distribution of the Cy5-labeled PS M/NPs in larval zebrafish. The data are presented as the mean ± SD (unless otherwise stated, $n = 3$ pools of 30 individuals per pool). Statistical comparisons were performed using ANOVA followed by Tukey's method. Data in Figure 8A,B,D,E,H,K,G,I are also presented in Excel Table S8. Unless otherwise stated, the concentrations for single or combined exposures are as follows: AgNPs: 10 μg/L; $AgNO_3$: 2.2 μg/L; PSNPs: 200 μg/L; PSMPs: 200 μg/L. The experimental subjects: Tg(*elavl3*: EGFP) transgenic zebrafish (the right column in C and E); AB wild-type zebrafish (all images except the right column in C and E). Note: AgNPs, silver nanoparticles; ANOVA, analysis of variance; EGFP, enhanced green fluorescent protein; *elavl3*, embryonic lethal, abnormal vision, *Drosophila*-like 3; hpf, hours post fertilization; PSMPs, polystyrene microspheres; PSNPs, polystyrene nanospheres; ROS, reactive oxygen species; SD, standard deviation. Significance levels: $^{*}p < 0.05$, $^{**}p < 0.01$, and $^{***}p < 0.001$.

In vitro adsorption analysis and TEM observation have elucidated the interactions between AgNPs and PS M/NPs. These interactions were likely driven by the phenyl or electrostatic forces of PS M/NPs, which are instrumental in the formation of PS M/NPs–AgNPs complexes.[35] Notably, MPs exhibited a pronounced affinity for AgNPs adsorption, a phenomenon that was intricately linked to the particle size of MPs.[50] This phenomenon may be attributed to the smaller size of MPs, which resulted in a

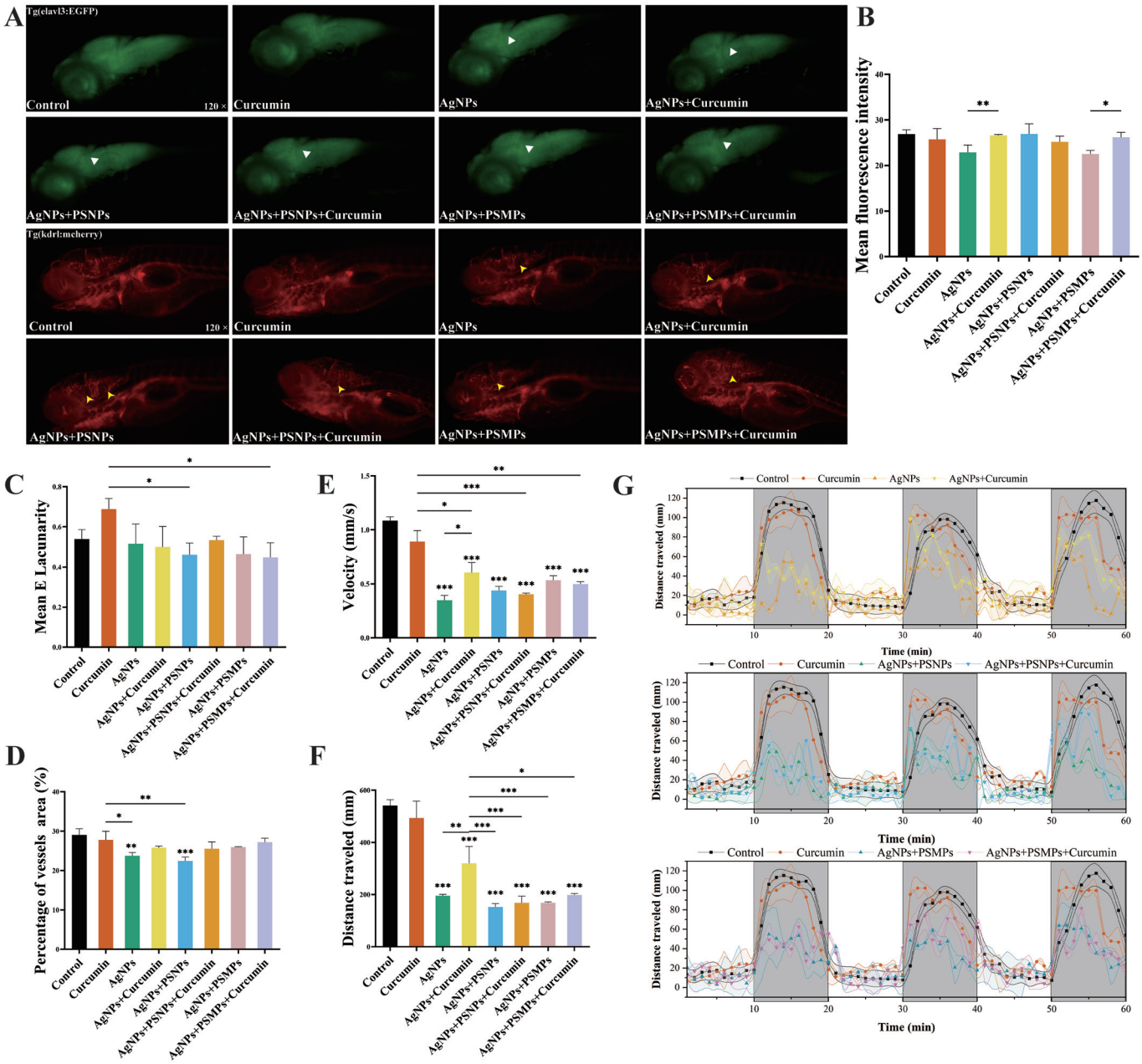

Figure 9. The effects of curcumin on zebrafish larvae exposed to control, AgNPs, or a combination of AgNPs with either PSNPs or PSMPs with and without curcumin treatment. (A) Differences in expression of *elavl3* in Tg(*elavl3*:EGFP) transgenic zebrafish at 96 hpf with and without rescue treatment with curcumin. (B) The qualification of the fluorescence expression changes of *elavl3*. (C) Vascular observation in Tg(*kdrl*:mCherry) transgenic zebrafish larvae observed at 96 hpf. (D,E) Vascular network analysis including porosity (D) and percentage area of blood vessels (E). (F,G) The quantification of velocity (F) and movement distance (G) in autonomous motion of larval zebrafish. (H) The movement distance of larval zebrafish subjected a 60-min dark-to-light photoperiod transition. The data are presented as the mean ± SD (unless otherwise stated, $n = 3$ pools of 30 individuals per pool). Statistical comparisons were performed using ANOVA followed by Tukey's method. Data in Figure 9B–H are also presented in Excel Table S9. Unless otherwise stated, the concentrations for single or combined exposures are as follows: AgNPs: 10 μg/L; PSNPs: 200 μg/L; PSMPs: 200 μg/L; curcumin: 200 μg/L. The experimental subjects: Tg(*elavl3*:EGFP) transgenic zebrafish (A and B); Tg(*kdrl*:mCherry) transgenic zebrafish (C–E); AB wild-type zebrafish (F–H). Note: AgNPs, silver nanoparticles; ANOVA analysis of variance; EGFP, enhanced green fluorescent protein; *elavl3*, embryonic lethal; abnormal vision, *Drosophila*-like 3; hpf, hours post fertilization; *kdrl*, kinase insert domain receptor-like; mCherry, monomeric Cherry; PSMPs, polystyrene microspheres; PSNPs, polystyrene nanospheres; SD, standard deviation. Significance levels: $^{*}p < 0.05$, $^{**}p < 0.01$, and $^{***}p < 0.001$.

larger surface area and a greater number of binding sites, thereby facilitating a more effective interaction with AgNPs.[51,52]

The chorionic membrane of the zebrafish embryo constitutes a distinctive biological barrier, safeguarding the developing organism from diverse pollutants. This membrane, punctuated with pores ranging from 500 to 700 nm, facilitates the transit of nanoparticles, salt ions, and essential oxygen.[53] *In vivo* research by Zhou et al.[54] showed that PSNPs as small as 8 nm and 24 nm were able to penetrate the chorionic membrane, gaining entry into the yolk sac. Conversely, larger PSMPs of up to 1,000 nm demonstrated a propensity to adhere robustly to the surface of the cell membrane, unable to permeate the chorionic barrier.[54] This suggested that varying sizes of MPs may have different uptake mechanisms, as demonstrated by the investigation of Cy5-labeled PS M/NPs uptake in embryos and larval zebrafish. In this study, at 24 hpf, the high uptake efficiency observed for Cy5-labeled

PSNPs indicated that both PSNPs and AN were internalized by the embryos, potentially inducing embryonic yolk cysts. During this period, the embryonic blood–brain barrier is undergoing development.[55] We expect that this may be the reason that AgNPs, PSNPs, and AN were able to access the cranial regions of the embryo, potentially impacting neural development. However, the toxicity of AgNPs was somewhat mitigated in the AM group prior to the hatching of embryos. By 96 hpf, the larvae were capable of autonomous movement and respiration. The ability to respire may have facilitated the uptake of larger PSMPs and AgNPs by zebrafish, increasing the toxicity observed in the AM group at 96 hpf, characterized by delayed swim bladder development, similar to the effects observed in the AgNPs exposure group. In the AN group, PSNPs facilitated the accumulation and transport of AgNPs within zebrafish, as confirmed by the measurement of Ag content in the organisms. The higher Ag accumulation in the zebrafish larvae may result in increased developmental toxicity.[56] This phenomenon was corroborated by empirical measurements of heart rate, muscular twitching, and body length.

Small NPs were capable of penetrating the chorionic membrane and blood–brain barrier of zebrafish embryos,[57] suggesting that the mechanisms of neurotoxicity in combined exposures may differ, potentially leading to varied behavioral responses in zebrafish. In autonomous movement assays, both AN and AM treatment groups exhibited significantly shorter movement distances in comparison with AgNPs exposure alone, despite exhibiting higher swimming speeds. PSNPs could carry substantial amounts of AgNPs into the larvae, releasing them at specific sites, thereby intensifying the toxicity of AgNPs. Because PSMPs were unable to penetrate the chorionic membrane and blood–brain barrier, they likely predominantly entered zebrafish larvae through gills and mouth during respiration, accumulating extensively in the digestive organs and altering the bioavailability of AgNPs. The indigestibility of PSMPs could adversely affect larval development, leading to an energy imbalance and a consequent shorter movement distance.[58,59] Tracking and heat maps also indicated that combined exposures altered neurophysiological responses in larval zebrafish, which may further result in stereotypical behaviors, stress, and depressive tendencies. This finding could explain why combined exposures exhibited greater movement speed but shorter travel distance compared with AgNPs exposure alone. The effect of PS M/NPs on the bioavailability of AgNPs was also reflected in differences in larval turning angles and photoperiod movement distances, where coexposure to PS M/NPs induced significantly more pronounced behavioral differences than exposure to AgNPs alone, including greater restlessness and erratic turning behavior. The coexposure of PSNPs and AgNPs weakened the perception of zebrafish to light–dark transitions when compared with the AgNPs exposure group, whereas AM showed an opposite effect to AN. These findings suggest that AN intensified the AgNPs-induced disruption of the light–dark adaptation regulatory mechanisms, primarily governed by retinal ganglion cells,[60] whereas AM exposure tended to counteract this disruption. This was primarily due to the different ways PSNPs and PSMPs altered the bioavailability of AgNPs. In addition, touch response experiments indicated that combined exposure to PS M/NPs led to delayed touch responses in zebrafish larvae, shorter movement duration, and excessive twitching. Overall, the behavioral results support the hypothesis that PS M/NPs altered the bioavailability of AgNPs, leading to various abnormal behaviors, and these effects were dependent on the particle size of M/NPs.

The relationship between vascular and neural networks is critical, particularly regarding the role of intracranial vascular system in the development of CNS. In osteichthyans and mammals, the cranial vascular system developed from a primitive plexus through angioblast migration and coalescence before the formation of the blood–brain barrier.[61] Angiogenesis is crucial for nutrient delivery to developing neural cells and CNS maturation.[62] Any disruptions in this process can lead to abnormal vascular connections, compromised integrity, intracranial aneurysms, and neuronal degeneration.[61] To further elucidate the potential mechanisms of combined exposure-mediated neurotoxicity, two transgenic zebrafish lines [Tg(*elavl3*:EGFP) and Tg(*kdrl*:mCherry)] were used to study the damage to the neural and cranial vasculature in larval zebrafish. The results indicated that combined exposure exacerbated the reduction in nascent neurons and vascular ablation. These findings suggest that the combined exposure to PS M/NPs with AgNPs significantly exacerbated the injury to intracranial vascular development triggered by AgNPs in zebrafish. Studies showed that external contaminants inhibiting AChE can cause ACh accumulation, leading to abnormal motor behaviors in zebrafish embryos.[63] The significantly lower AChE activity further suggests that combined exposure exerted a stronger neurotoxic effect. Moreover, this exposure resulted in different expressions of vascular marker genes (*kdrl* and *fli1a*) from control zebrafish, consistent with observations in the aforementioned Tg(*kdrl*:mCherry) zebrafish. These findings suggest that AgNPs exposure induced neuro- and vascular toxicity in zebrafish, with this toxicity exacerbated in combination with PSNPs but less affected by coexposure with PSMPs. The variation in toxicity may primarily be attributed to the differences in uptake rates and AgNPs adsorption scenarios, influenced by the distinct particle sizes of PS M/NPs. Our uptake experiments showed that zebrafish internalized PSNPs far more efficiently than PSMPs, whereas adsorption tests indicated that PSNPs also adsorbed AgNPs more effectively. Consequently, Ag accumulation was higher in the AN group than that in the AM group, as confirmed by Ag content measurements.

The primary mechanism of toxicity of nanomaterials is believed to be through the induction of oxidative stress in organisms, typically arising from an imbalance in oxidative states caused by exogenous substances.[55] By assessing differences in ROS, MDA, and GSH under combined exposure, we demonstrated that such exposure induced oxidative stress in larval zebrafish, with both PSNPs and PSMPs exacerbating the oxidative stress induced by AgNPs. As the level of oxidative stress within the body becomes higher, it may lead to cellular apoptosis and activation of immune responses. The interaction between neurons and immune cells is crucial for homeostasis and species survival, with immune cell activation influencing neuronal circuits that govern immunity.[64] In fish, the innate immune system functions independently in early development, maturing fully in later juvenile stages (4–6 wk).[65,66] Consequently, the innate immune system, critical in early zebrafish development, provides essential defense against pathogens. Within this system, macrophages emerge as key agents in the regeneration of the injured peripheral nervous system.[67] Observations of differences in Tg(*coro1a*:EGFP) fluorescence intensity and the quantity of macrophages post neutral red staining under combined exposure support the idea that this exposure disrupted the innate immune system in larval zebrafish, resulting in significant immune cell accumulation. The AN group, in comparison with the AgNPs and AM groups, showed the most significant immune cell aggregation around the zebrafish neural system, indicating a robust immune response and a greater neuroinflammatory response.[68] Apoptosis is a crucial biological process in embryogenesis, tissue homeostasis, and immune system regulation.[69] AO apoptotic staining results further suggest that PS M/NPs exacerbated the damage caused by AgNPs to the zebrafish neural system. *Caspase3*, essential for

apoptosis and cytotoxic T lymphocyte activity, is vital in programmed cell death, whereas *caspase9*, a pro-apoptotic factor, is crucial for initiating apoptosis.[70,71] *Tnfα*, a macrophage-secreted cytokine integral to systemic inflammation, modulates immune cell secretion and induces apoptosis,[72] playing a pivotal role in inflammatory and autoimmune disorders.[73,74] *Il10*, as a key regulator in immune responses, potentially exerts a profound influence on diseases marked by heightened inflammation, particularly in cancer and infectious disease scenarios.[75,76] The significant up-regulation of immune-related genes (*il10* and *tnf-α*) and apoptosis-related genes (*caspase3* and *caspase9*) under combined exposure further supports the potential of combined exposure to induce dysfunction in the neuroimmune system.

At the molecular level, the neuronal differentiation marker genes (*pax6a*, *elavl3*, *ptafr*, and *egr2b*) and synaptic regeneration marker genes (*gabbr1a* and *gabbr1b*) were selected to explore the potential mechanism of combined exposure. *Pax6a*, a brain marker gene instrumental in nervous system development, exhibits widespread expression across various brain regions of zebrafish.[76] *Elavl3*, a neurodevelopmental marker, is intimately linked with vertebrate neuronal differentiation and maturation.[77] *Egr2b* plays a crucial role in cell growth, differentiation, and apoptosis, and it is implicated in various immune disorders and early onset neuropathies in zebrafish.[78] The platelet-activating factor receptor (*ptafr*) is notable for its high expression in microglia and brain tissues in Alzheimer disease (AD) patients.[79] *Gabbr1a* and *gabbr1b*, gamma-aminobutyric acid (GABA) B receptor genes, are associated with neuroplasticity, regulating neuronal synaptogenesis and implicated in numerous neurological disorders in patients.[80] The differences in the expression of these above genes under combined exposure suggests that combined exposure to PS M/NPs of different particle sizes and AgNPs could affect neuron generation and synaptic regeneration, with distinct mechanisms of toxic effects. However, more studies with functional end points are needed to make this conclusion. These differences in gene expressions may partly explain the observed behavioral abnormalities and developmental neurotoxicity in zebrafish exposed to different particle-sized PS M/NPs combined with AgNPs. The higher expression of *ptafr* and *egr2b* genes[79,81] after exposure to PSNPs indicate a potential for more severe neural damage. The differential expression of neural-related genes observed among the AgNPs, AM, and AN groups could underlie the varying degrees of neurotoxicity associated with combined exposure, with the AN group showing particularly pronounced effects, as demonstrated by abnormal gene expression profiles.

Furthermore, the combined effects of AgNPs and PS MPs/NPs on neuroinflammation were further assessed, indicating that exposures exhibited synergistic interactions with regard to most biomarkers. The joint toxicity of AgNPs and PSNPs was significantly stronger than that of AgNPs alone. Because of the nonlinear cumulative nature of synergistic effects, even when individual pollutant concentrations were below their toxicity thresholds, combined exposure may still pose health risks. Thus, this finding is crucial for risk assessments of micoplastics and other nanomaterials at environmentally relevant concentrations.

Considering that AgNPs underwent oxidative dissolution in water, leading to the production of toxic Ag^+ *in vitro*,[82] we aimed to investigate whether the neurotoxicity induced by AgNPs and AM/AN was primarily due to the release of Ag^+ or the nanoparticles themselves. Based on the dissolution profile of AgNPs, $\sim 22\%$ of Ag^+ was released after 24 h. However, in the presence of PS M/NPs, the release rate of Ag^+ was significantly lower, with the lowest release observed in the AN group. To further explore this, zebrafish were exposed to $AgNO_3$ at concentrations equivalent to the 24-h Ag^+ release from AgNPs, and their neurotoxic effects were assessed. The results showed that the accumulation of AgNPs in zebrafish larvae was significantly higher than that of Ag^+ alone. Moreover, the Ag accumulations in both AM and AN groups were considerably higher than that in the AgNPs group. This suggested that, in addition to Ag^+, AgNPs were taken up by zebrafish in particle form. Furthermore, the significantly lower release of Ag^+ in the coexposure groups (AM and AN), combined with higher Ag accumulation, further supports this finding. In addition, in comparison with the $AgNO_3$ group, AgNPs exhibited stronger oxidative stress, greater inhibition of neuronal cell proliferation, poorer swimming activity, and lower sensitivity to light–dark stimuli, indicating that the neurotoxicity induced by AgNPs was not solely attributable to Ag^+ but also to the particulate nature of AgNPs themselves. To investigate why Ag accumulations in the AM and AN groups were significantly higher than that in the AgNPs group, we assessed the uptake of PS M/NPs in zebrafish. At 24 hpf, PSMPs, presumably due to their larger size, primarily accumulated in the chorion. By 72 hpf, they were detected in the larvae, with uptake increasing over time, eventually leading to accumulation in the intestines, pancreas, and other organs by 120 hpf. In contrast, PSNPs were absorbed by embryos as early as 24 hpf, with significantly higher uptake than PSMPs. Therefore, we infer that the adsorption of AgNPs onto PS M/NPs facilitated the aggregation of AgNPs, whereas PS M/NPs themselves were also taken up by zebrafish, leading to significant Ag accumulation in the organisms. The greater toxicity observed in the AN group may also be attributed to the higher uptake efficiency of PSNPs.

According to these results, combined exposure to AgNPs and PS M/NPs intensified oxidative stress, inflammatory responses, cell apoptosis, and neurovascular damage. Curcumin is an effective neuroprotectant known for its antioxidative, anti-inflammatory, and antineuronal apoptosis properties.[83] This compound played a significant role in ameliorating chronic neurodegenerative disorders by promoting mitochondrial biogenesis *in vivo*.[84] Its neuroprotective efficacy largely stemmed from its capacity to alleviate oxidative neural damage, attenuate inflammatory responses, and finely regulate metabolic processes,[85] which may counteract the neurotoxicity caused by AgNPs and combined exposure. The incorporation of curcumin markedly ameliorated the impairment in neural and vascular development, alongside leading to stronger autonomous motility and a more regular circadian rhythm, in comparison with groups without curcumin treatment. This observation supports our hypothesis that curcumin exerted a therapeutic influence on AgNPs-induced neurotoxicity, with its efficacy being most pronounced in the AgNPs group, followed by the AM and AN groups. This differential effect may be attributed to the encapsulation of AgNPs by curcumin, leading to the formation of curcumin–AgNPs complexes, which mitigated the inherent toxicity of AgNPs. Given the robust adsorptive affinity of PS M/NPs toward AgNPs, which altered their bioavailability, the quantity of AgNPs adsorbed onto the surface of PSNPs surpassed that on PSMPs. This significantly fewer available adsorptive sites on PSNPs may have consequently impeded the effective use of curcumin by zebrafish, thereby diminishing its therapeutic impact in the AN group. In summary, coexposure to PS M/NPs and AgNPs demonstrated distinct neurotoxic mechanisms, with the presence of PS M/NPs also hindering the efficacy of therapeutic interventions. These observed effects were intricately linked to the particle size of the PS M/NPs involved. Further in-depth research is essential to comprehensively understand these specific toxicity mechanisms.

In rivers in Malaysia that receive various types of wastewater effluents, the concentrations of AgNPs have alarmingly escalated to a range between 0.1 and 10 mg/L.[29] In urban lakes, such as

those in Lubbock, Texas, microplastics concentrations have been measured at 1.56 ± 1.64 mg/L,[9] with PS microplastics accounting for 11.9% of the total microplastics in lake waters across the Americas.[85] Therefore, the concentration we chose in this study (AgNPs: 10 μg/L; PS M/NPs: 200 μg/L) was close to the real-world concentration. Recent studies have shown that microplastics and engineered nanomaterials, including AgNPs, share similar pathways (e.g., domestic sewage, wastewater treatment plants) into natural environments.[25,33] Notably, Li et al.[35] systematically investigated the coexposure of PSMPs and AgNPs in natural freshwater and brackish water, revealing that AgNPs could be captured and aggregated by PSMPs. Thus, investigating the environmental and biological impacts of coexposure to AgNPs and PS M/NPs at environmentally relevant concentrations is essential. Moreover, recognizing that the PSMPs used in this study do not capture the full diversity of environmental microplastics, we introduced additional MPs with distinct surface charges (e.g., PLA and PA MPs) as well as PSMPs with mixed particle sizes. Each type was coexposed with AgNPs to assess neurotoxicity in zebrafish and thereby validate the broad applicability of our findings. Our results showed that coexposure to PLA or PA MPs and AgNPs induced excessive oxidative stress, behavioral retardation, and disruptions in photoperiodic rhythms, though these effects were less severe than those caused by AgNPs alone. However, these adverse effects were more pronounced in the Mix + AgNPs group. This indicated that the combined exposure of PLA and PA with AgNPs resulted in weaker neurotoxicity than AgNPs alone, whereas the exposure of Mix + AgNPs led to stronger neurotoxicity than AgNPs alone. From the results above, it can be observed that the combined effects of MPs and AgNPs may be influenced more by the inherent chemical properties of MPs. In addition, when considering microplastics in real-world environments, the release of various plastic additives often accompanied them. Previous studies have detected additives such as BPA, diethylhexyl phthalate (DEHP), 2,4,6-tribromophenol (TBP), and tetrabromobisphenol A (TBBPA) in the leachates of PS microplastics.[86,87] However, because the exposure concentration of PS M/NPs selected in our study was below the NOEC threshold of 10 mg/L, the toxicity of additives released through leachates can be considered negligible in this study. Hence, a key focus of future research will be assessing the ecological risks of coexposure to AgNPs and microplastics with varying components, sizes, and shapes on organisms in real aquatic environments. Overall, these findings emphasize the need for comprehensive environmental risk assessments where such pollutants coexist. In addition, employing curcumin as a neurotoxicity mitigant suggests innovative strategies to counteract the effects of combined pollution, thereby proposing a method to diminish the ecological impact of these materials.

Conclusion

In general, this study revealed that the adsorptive interaction between PS M/NPs and AgNPs was heavily influenced by the particle size of the MPs, with smaller MPs exhibiting a higher adsorptive capability. Larval zebrafish coexposed to PS M/NPs and AgNPs exhibited a series of abnormalities, such as developmental deformities, aberrations in developmental and physiological markers, delayed tactile response, and abnormal behaviors. This exposure notably led to greater oxidative stress, disrupted neural and vascular development, lower AChE levels, and higher levels of cellular apoptosis in the zebrafish larval brain. In addition, qPCR analysis further established that the combined exposure induced differential gene expression associated with neural development, immune response, and apoptosis. These findings delineated how the combination of AgNPs with MPs of different sizes manifested distinct neurotoxic effects, with PSNPs significantly amplifying the neurotoxicity induced by AgNPs, in contrast to the milder impact of PSMPs. By comparing exposure to $AgNO_3$ at a concentration equivalent to the dissolved Ag^+ concentration from AgNPs after 24 h, it was found that the toxicity of AgNPs was not solely attributable to the release of silver ions but was also closely associated with the intrinsic toxicity of the nanoparticles themselves. The application of curcumin, known for its anti-neuroinflammatory properties, provided varying degrees of mitigation against the neurotoxicity induced by AgNPs and their combinations, indicating that the neurotoxicity from such combined exposures could stem from greater oxidative stress and neuroimmune activation. These insights are instrumental in framing the environmental risk assessment of microplatics and AgNPs and pave the way for future research on the joint toxicity of nanomaterials.

Acknowledgments

This work was jointly supported by the National Natural Science Foundation of China (22305167, 32071617, 32371705), and Natural Science Foundation of Jiangsu Province (BK20231341).

J.S.: conceptualization, investigation, data curation, writing original draft. Q.P.: formal analysis and methodology. C.C.: methodology. X.L.: data curation. X.Z.: data curation. Z.W.: review and editing. J.Y.: review and editing. X.W.: review and editing. H.W.: visualization, supervision, and funding acquisition. Q.Q.: conceptualization, supervision, review and editing, and funding acquisition.

This study was approved by the Ethics Committee of Suzhou University of Science and Technology, Suzhou, China.

References

1. Alimi OS, Farner Budarz J, Hernandez LM, Tufenkji N. 2018. Microplastics and nanoplastics in aquatic environments: aggregation, deposition, and enhanced contaminant transport. Environ Sci Technol 52(4):1704–1724, PMID: 29265806, https://doi.org/10.1021/acs.est.7b05559.
2. Rochman CM, Kross SM, Armstrong JB, Bogan MT, Darling ES, Green SJ, et al. 2015. Scientific evidence supports a ban on microbeads. Environ Sci Technol 49(18):10759–10761, PMID: 26334581, https://doi.org/10.1021/acs.est.5b03909.
3. Kim J-H, Yu Y-B, Choi J-H. 2021. Toxic effects on bioaccumulation, hematological parameters, oxidative stress, immune responses and neurotoxicity in fish exposed to microplastics: a review. J Hazard Mater 413:125423, PMID: 33930961, https://doi.org/10.1016/j.jhazmat.2021.125423.
4. Zhang C, Wang J, Zhou A, Ye Q, Feng Y, Wang Z, et al. 2021. Species-specific effect of microplastics on fish embryos and observation of toxicity kinetics in larvae. J Hazard Mater 403:123948, PMID: 33264992, https://doi.org/10.1016/j.jhazmat.2020.123948.
5. Strokal M, Vriend P, Bak MP, Kroeze C, van Wijnen J, van Emmerik T. 2023. River export of macro- and microplastics to seas by sources worldwide. Nat Commun 14(1):4842, PMID: 37563145, https://doi.org/10.1038/s41467-023-40501-9.
6. Lebreton LCM, van der Zwet J, Damsteeg J-W, Slat B, Andrady A, Reisser J. 2017. River plastic emissions to the world's oceans. Nat Commun 8(1):15611, PMID: 28589961, https://doi.org/10.1038/ncomms15611.
7. Lasee S, Mauricio J, Thompson WA, Karnjanapiboonwong A, Kasumba J, Subbiah S, et al. 2017. Microplastics in a freshwater environment receiving treated wastewater effluent. Integr Environ Assess Manag 13(3):528–532, PMID: 28440932, https://doi.org/10.1002/ieam.1915.
8. Portillo De Arbeloa N, Marzadri A. 2024. Modeling the transport of microplastics along river networks. Sci Total Environ 911:168227, PMID: 37977379, https://doi.org/10.1016/j.scitotenv.2023.168227.
9. Fan Y, Zheng K, Zhu Z, Chen G, Peng X. 2019. Distribution, sedimentary record, and persistence of microplastics in the Pearl River Catchment, China. Environ Pollut 251:862–870, PMID: 31234251, https://doi.org/10.1016/j.envpol.2019.05.056.
10. Yu Y, Chen H, Hua X, Dang Y, Han Y, Yu Z, et al. 2020. Polystyrene microplastics (PS-MPs) toxicity induced oxidative stress and intestinal injury in nematode *Caenorhabditis elegans*. Sci Total Environ 726:138679, PMID: 32320865, https://doi.org/10.1016/j.scitotenv.2020.138679.
11. Lu Y, Zhang Y, Deng Y, Jiang W, Zhao Y, Geng J, et al. 2016. Uptake and accumulation of polystyrene microplastics in zebrafish (*Danio rerio*) and toxic effects in liver. Environ Sci Technol 50(7):4054–4060, PMID: 26950772, https://doi.org/10.1021/acs.est.6b00183.

12. Hamed M, Martyniuk CJ, Naguib M, Lee J-S, Sayed A-DH. 2022. Neurotoxic effects of different sizes of plastics (nano, micro, and macro) on juvenile common carp (*Cyprinus carpio*). Front Mol Neurosci 15:1028364, PMID: 36340695, https://doi.org/10.3389/fnmol.2022.1028364.
13. Yu H, Chen Q, Qiu W, Ma C, Gao Z, Chu W, et al. 2022. Concurrent water- and foodborne exposure to microplastics leads to differential microplastic ingestion and neurotoxic effects in zebrafish. Water Res 219:118582, PMID: 35580390, https://doi.org/10.1016/j.watres.2022.118582.
14. Santana-Viera S, Montesdeoca-Esponda S, Guedes-Alonso R, Sosa-Ferrera Z, Santana-Rodríguez JJ. 2021. Organic pollutants adsorbed on microplastics: analytical methodologies and occurrence in oceans. Trends Environ Anal Chem 29: e00114, https://doi.org/10.1016/j.teac.2021.e00114.
15. Lobelle D, Cunliffe M. 2011. Early microbial biofilm formation on marine plastic debris. Mar Pollut Bull 62(1):197–200, PMID: 21093883, https://doi.org/10.1016/j.marpolbul.2010.10.013.
16. Yu F, Yang C, Zhu Z, Bai X, Ma J. 2019. Adsorption behavior of organic pollutants and metals on micro/nanoplastics in the aquatic environment. Sci Total Environ 694:133643, PMID: 31756812, https://doi.org/10.1016/j.scitotenv.2019.133643.
17. Bakir A, Rowland SJ, Thompson RC. 2014. Transport of persistent organic pollutants by microplastics in estuarine conditions. Estuarine Coastal Shelf Sci 140:14–21, https://doi.org/10.1016/j.ecss.2014.01.004.
18. Zhao L, Rong L, Xu J, Lian J, Wang L, Sun H. 2020. Sorption of five organic compounds by polar and nonpolar microplastics. Chemosphere 257:127206, PMID: 32502737, https://doi.org/10.1016/j.chemosphere.2020.127206.
19. Rios-Fuster B, Alomar C, Paniagua González G, Garcinuño Martínez R, Soliz Rojas D, Fernández Hernando P, et al. 2022. Assessing microplastic ingestion and occurrence of bisphenols and phthalates in bivalves, fish and holothurians from a Mediterranean marine protected area. Environ Res 214(pt 3):114034, PMID: 35948144, https://doi.org/10.1016/j.envres.2022.114034.
20. Han Y, Shi W, Tang Y, Zhou W, Sun H, Zhang J, et al. 2022. Microplastics and bisphenol a hamper gonadal development of whiteleg shrimp (*Litopenaeus vannamei*) by interfering with metabolism and disrupting hormone regulation. Sci Total Environ 810:152354, PMID: 34914981, https://doi.org/10.1016/j.scitotenv.2021.152354.
21. Sheng C, Zhang S, Zhang Y. 2021. The influence of different polymer types of microplastics on adsorption, accumulation, and toxicity of triclosan in zebrafish. J Hazard Mater 402:123733, PMID: 33254764, https://doi.org/10.1016/j.jhazmat.2020.123733.
22. Ding C, Chen J, Zhu F, Chai L, Lin Z, Zhang K, et al. 2022. Biological toxicity of heavy metal(loid)s in natural environments: from microbes to humans. Front Environ Sci 10, https://doi.org/10.3389/fenvs.2022.920957.
23. He B, Liu A, Duodu GO, Wijesiri B, Ayoko GA, Goonetilleke A. 2023. Distribution and variation of metals in urban river sediments in response to microplastics presence, catchment characteristics and sediment properties. Sci Total Environ 856(pt 2):159139, PMID: 36191715, https://doi.org/10.1016/j.scitotenv.2022.159139.
24. Gao F, Li J, Sun C, Zhang L, Jiang F, Cao W, et al. 2019. Study on the capability and characteristics of heavy metals enriched on microplastics in marine environment. Mar Pollut Bull 144:61–67, PMID: 31180007, https://doi.org/10.1016/j.marpolbul.2019.04.039.
25. Hüffer T, Praetorius A, Wagner S, von der Kammer F, Hofmann T. 2017. Microplastic exposure assessment in aquatic environments: learning from similarities and differences to engineered nanoparticles. Environ Sci Technol 51(5):2499–2507, PMID: 28125881, https://doi.org/10.1021/acs.est.6b04054.
26. He Q, Lu J, Liu N, Lu W, Li Y, Shang C, et al. 2022. Antiviral properties of silver nanoparticles against SARS-CoV-2: effects of surface coating and particle size. Nanomaterials (Basel) 12(6):990, PMID: 35335803, https://doi.org/10.3390/nano12060990.
27. De-la-Torre GE, Dioses-Salinas DC, Pizarro-Ortega CI, Fernández Severini MD, Forero López AD, Mansilla R, et al. 2022. Binational survey of personal protective equipment (PPE) pollution driven by the COVID-19 pandemic in coastal environments: abundance, distribution, and analytical characterization. J Hazard Mater 426:128070, PMID: 34922133, https://doi.org/10.1016/j.jhazmat.2021.128070.
28. Xiao B, Zhang Y, Wang X, Chen M, Sun B, Zhang T, et al. 2019. Occurrence and trophic transfer of nanoparticulate Ag and Ti in the natural aquatic food web of Taihu Lake, China. Environ Sci: Nano 6(11):3431–3441, https://doi.org/10.1039/C9EN00797K.
29. Syafiuddin A, Salmiati S, Hadibarata T, Kueh ABH, Salim MR, Zaini MAA. 2018. Silver nanoparticles in the water environment in Malaysia: inspection, characterization, removal, modeling, and future perspective. Sci Rep 8(1):986, PMID: 29343711, https://doi.org/10.1038/s41598-018-19375-1.
30. Seyedi J, Tayemeh M, Esmaeilbeigi M, Joo H, Langeroudi E, Banan A, et al. 2021. Fatty acid alteration in liver, brain, muscle, and oocyte of zebrafish (*Danio rerio*) exposed to silver nanoparticles and mitigating influence of quercetin-supplemented diet. Environ Res 194:110611, PMID: 33358875, https://doi.org/10.1016/j.envres.2020.110611.
31. Yan N, Wang W. 2022. Maternal transfer and biodistribution of citrate and luminogens coated silver nanoparticles in medaka fish. J Hazard Mater 433:128862, PMID: 35398793, https://doi.org/10.1016/j.jhazmat.2022.128862.
32. Dąbrowska-Bouta B, Sulkowski G, Gewartowska M, Strużyńska L. 2022. Endoplasmic reticulum stress underlies nanosilver-induced neurotoxicity in immature rat brain. Int J Mol Sci 23(21):13013, PMID: 36361797, https://doi.org/10.3390/ijms232113013.
33. Potter PM, Navratilova J, Rogers KR, Al-Abed SR. 2019. Transformation of silver nanoparticle consumer products during simulated usage and disposal. Environ Sci Nano 6(2):592–598, PMID: 31728194.
34. Kutralam-Muniasamy G, Pérez-Guevara F, Shruti VC. 2022. A critical synthesis of current peer-reviewed literature on the environmental and human health impacts of COVID-19 PPE litter: new findings and next steps. J Hazard Mater 422:126945, PMID: 34449351, https://doi.org/10.1016/j.jhazmat.2021.126945.
35. Li P, Zou X, Wang X, Su M, Chen C, Sun X, et al. 2020. A preliminary study of the interactions between microplastics and citrate-coated silver nanoparticles in aquatic environments. J Hazard Mater 385:121601, PMID: 31727533, https://doi.org/10.1016/j.jhazmat.2019.121601.
36. Jia R, Zhang Y, Wang Y, Wang Y, Sun G, Jiang Y. 2024. Toxic effects on ciliates under nano-/micro-plastics coexist with silver nanoparticles. J Hazard Mater 465:133058, PMID: 38006860, https://doi.org/10.1016/j.jhazmat.2023.133058.
37. de Esch C, Slieker R, Wolterbeek A, Woutersen R, de Groot D. 2012. Zebrafish as potential model for developmental neurotoxicity testing: a mini review. Neurotoxicol Teratol 34(6):545–553, PMID: 22971930, https://doi.org/10.1016/j.ntt.2012.08.006.
38. Tropepe V, Sive HL. 2003. Can zebrafish be used as a model to study the neurodevelopmental causes of autism? Genes Brain Behav 2(5):268–281, PMID: 14606692, https://doi.org/10.1034/j.1601-183x.2003.00038.x.
39. Wu X, Shen W, Zhang B, Meng A. 2018. The genetic program of oocytes can be modified *in vivo* in the zebrafish ovary. J Mol Cell Biol 10(6):479–493, PMID: 30060229, https://doi.org/10.1093/jmcb/mjy044.
40. Wang C, Hui J, Zhu X-h, Cui S-y, Cui Z-M, Xu D. 2020. Lobetyolin efficiently promotes angiogenesis and neuronal development in transgenic zebrafish. Nat Prod Commun 15(8), https://doi.org/10.1177/1934578X20937174.
41. Li L, Yan B, Shi YQ, Zhang WQ, Wen ZL. 2012. Live imaging reveals differing roles of macrophages and neutrophils during zebrafish tail fin regeneration. J Biol Chem 287(30):25353–25360, PMID: 22573321, https://doi.org/10.1074/jbc.M112.349126.
42. Wu D, Wang T, Wang J, Jiang L, Yin Y, Guo H. 2021. Size-dependent toxic effects of polystyrene microplastic exposure on microcystis aeruginosa growth and microcystin production. Sci Total Environ 761:143265, PMID: 33257060, https://doi.org/10.1016/j.scitotenv.2020.143265.
43. Ling Y, Sun L, Wang D, Jiang J, Sun W, Ai W, et al. 2020. Triclosan induces zebrafish neurotoxicity by abnormal expression of miR-219 targeting oligodendrocyte differentiation of central nervous system. Arch Toxicol 94(3):857–871, PMID: 32060586, https://doi.org/10.1007/s00204-020-02661-1.
44. Umeda K, Shoji W. 2017. From neuron to behavior: sensory-motor coordination of zebrafish turning behavior. Dev Growth Differ 59(3):107–114, PMID: 28326550, https://doi.org/10.1111/dgd.12345.
45. Qiao R, Lu K, Deng Y, Ren H, Zhang Y. 2019. Combined effects of polystyrene microplastics and natural organic matter on the accumulation and toxicity of copper in zebrafish. Sci Total Environ 682:128–137, PMID: 31117014, https://doi.org/10.1016/j.scitotenv.2019.05.163.
46. Liu H, Jang J, French AS, Torkkeli PH. 2024. Sequence analysis, homology modeling, tissue expression, and potential functions of seven putative acetylcholinesterases in the spider *Cupiennius salei*. Eur J Neurosci 60(7):5785–5811, PMID: 39230060, https://doi.org/10.1111/ejn.16524.
47. Bhalerao A, Summers P. 2001. *Angiotool: A Tool for Interactive Visualization of MRI Vector and Tensor Fields*. Coventry, UK: University of Warwick.
48. Fan Y, Jiaping W, Huangyingzi W, Yinzhou B, Haoyu X, Wenpei Y, et al. 2024. Interaction of microplastics with perfluoroalkyl and polyfluoroalkyl substances in water: a review of the fate, mechanisms and toxicity. Sci Total Environ 948(0):175000, PMID: 39053539, https://doi.org/10.1016/j.scitotenv.2024.175000.
49. Weike S, Lu S, Yujie G, Hongli J, Wusu W, Lin Y, et al. 2024. Sight of aged microplastics adsorbing heavy metal exacerbated intestinal injury: a mechanistic study of autophagy-mediated toxicity response. ACS Nano 18(42):28849–28865, PMID: 39392295, https://doi.org/10.1021/acsnano.4c08737.
50. Wang Z, Chen M, Zhang L, Wang K, Yu X, Zheng Z, et al. 2018. Sorption behaviors of phenanthrene on the microplastics identified in a mariculture farm in Xiangshan Bay, southeastern China. Sci Total Environ 628-629:1617-1626, PMID: 30045578, https://doi.org/10.1016/j.scitotenv.2018.02.146.
51. Nguyen TB, Ho TB, Huang CP, Chen CW, Chen WH, Hsieh S, et al. 2022. Adsorption of lead(II) onto PE microplastics as a function of particle size: influencing factors and adsorption mechanism. Chemosphere 304:135276, PMID: 35690170, https://doi.org/10.1016/j.chemosphere.2022.135276.
52. Munoz M, Ortiz D, Nieto-Sandoval J, de Pedro ZM, Casas JA. 2021. Adsorption of micropollutants onto realistic microplastics: role of microplastic nature, size, age, and NOM fouling. Chemosphere 283:131085, PMID: 34146885, https://doi.org/10.1016/j.chemosphere.2021.131085.
53. Pitt J, Kozal J, Jayasundara N, Massarsky A, Trevisan R, Geitner N, et al. 2018. Uptake, tissue distribution, and toxicity of polystyrene nanoparticles in

developing zebrafish (*Danio rerio*). Aquat Toxicol 194:185–194, PMID: 29197232, https://doi.org/10.1016/j.aquatox.2017.11.017.
54. Zhou R, Zhou D, Yang S, Shi Z, Pan H, Jin Q, et al. 2023. Neurotoxicity of polystyrene nanoplastics with different particle sizes at environment-related concentrations on early zebrafish embryos. Sci Total Environ 872:162096, PMID: 36791853, https://doi.org/10.1016/j.scitotenv.2023.162096.
55. Legradi J, Di Paolo C, Kraak M, van der Geest H, Schymanski E, Williams A, et al. 2018. An ecotoxicological view on neurotoxicity assessment. Environ Sci Eur 30(1):46, PMID: 30595996, https://doi.org/10.1186/s12302-018-0173-x.
56. Cao H, Guo Y, Ma C, Wang Y, Jing Y, Chen X, et al. 2024. Comparative study of the effects of different surface-coated silver nanoparticles on thyroid disruption and bioaccumulation in zebrafish early life. Chemosphere 360:142422, PMID: 38795916, https://doi.org/10.1016/j.chemosphere.2024.142422.
57. Karkossa I, Bannuscher A, Hellack B, Wohlleben W, Laloy J, Stan MS, et al. 2021. Nanomaterials induce different levels of oxidative stress, depending on the used model system: comparison of *in vitro* and *in vivo* effects. Sci Total Environ 801:149538, PMID: 34428663, https://doi.org/10.1016/j.scitotenv.2021.149538.
58. Ruthsatz K, Schwarz A, Gomez-Mestre I, Meyer R, Domscheit M, Bartels F, et al. 2023. Life in plastic, it's not fantastic: sublethal effects of polyethylene microplastics ingestion throughout amphibian metamorphosis. Sci Total Environ 885:163779, PMID: 37146798, https://doi.org/10.1016/j.scitotenv.2023.163779.
59. Gardon T, Reisser C, Soyez C, Quillien V, Le Moullac G. 2018. Microplastics affect energy balance and gametogenesis in the pearl oyster *Pinctada margaritifera*. Environ Sci Technol 52(9):5277–5286, PMID: 29620881, https://doi.org/10.1021/acs.est.8b00168.
60. Mure LS, Vinberg F, Hanneken A, Panda S. 2019. Functional diversity of human intrinsically photosensitive retinal ganglion cells. Science 366(6470):1251–1255, PMID: 31806815, https://doi.org/10.1126/science.aaz0898.
61. Kugler E, Snodgrass R, Bowley G, Plant K, Serbanovic-Canic J, Hamilton N, et al. 2021. The effect of absent blood flow on the zebrafish cerebral and trunk vasculature. Vasc Biol 3(1):1–16, PMID: 34522840, https://doi.org/10.1530/VB-21-0009.
62. Eisa-Beygi S, Benslimane F, El-Rass S, Prabhudesai S, Abdelrasoul M, Simpson P, et al. 2018. Characterization of endothelial cilia distribution during cerebral-vascular development in zebrafish (*Danio rerio*). Arterioscler Thromb Vasc Biol 38(12):2806–2818, PMID: 30571172, https://doi.org/10.1161/ATVBAHA.118.311231.
63. Wang H, Meng Z, Liu F, Zhou L, Su M, Meng Y, et al. 2020. Characterization of boscalid-induced oxidative stress and neurodevelopmental toxicity in zebrafish embryos. Chemosphere 238:124753, PMID: 31545217, https://doi.org/10.1016/j.chemosphere.2019.124753.
64. Chavan SS, Pavlov VA, Tracey KJ. 2017. Mechanisms and therapeutic relevance of neuro-immune communication. Immunity 46(6):927–942, PMID: 28636960, https://doi.org/10.1016/j.immuni.2017.06.008.
65. Rosowski EE. 2020. Determining macrophage versus neutrophil contributions to innate immunity using larval zebrafish. Dis Model Mech 13(1):1684, PMID: 31932292, https://doi.org/10.1242/dmm.041889.
66. Rodgers ML, Simning D, Sepúlveda MS, De Guise S, Bosker T, Griffitt RJ. 2020. Exposure to oil and hypoxia results in alterations of immune transcriptional patterns in developing sheepshead minnows (*Cyprinodon variegatus*). Sci Rep 10(1):1684, PMID: 32015368, https://doi.org/10.1038/s41598-020-58171-8.
67. Salvador AFM, Kipnis J. 2022. Immune response after central nervous system injury. Semin Immunol 59:101629, PMID: 35753867, https://doi.org/10.1016/j.smim.2022.101629.
68. Zhang W, Xiao D, Mao Q, Xia H. 2023. Role of neuroinflammation in neurodegeneration development. Signal Transduct Target Ther 8(1):267, PMID: 37433768, https://doi.org/10.1038/s41392-023-01486-5.
69. Rathmell JC, Thompson CB. 2002. Pathways of apoptosis in lymphocyte development, homeostasis, and disease. Cell 109 Suppl:S97–S107, PMID: 11983156, https://doi.org/10.1016/s0092-8674(02)00704-3.
70. Shi X, Li M, Huang Q, Xie L, Huang Z. 2023. Monacolin k induces apoptosis of human glioma U251 cells by triggering ROS-mediated oxidative damage and regulating MAPKs and NFκB pathways. ACS Chem Neurosci 14(7):1331–1341, PMID: 36917811, https://doi.org/10.1021/acschemneuro.3c00104.
71. Sandoval A, Vaughn L, Huang J, Barbieri J. 2023. Role of tumor necrosis factor-α inhibitors in the treatment and occurrence of acne: a systematic review. JAMA Dermatol 159(5):504–509, PMID: 36930143, https://doi.org/10.1001/jamadermatol.2023.0269.
72. Sedger LM, McDermott MF. 2014. TNF and TNF-receptors: from mediators of cell death and inflammation to therapeutic giants – past, present and future. Cytokine Growth Factor Rev 25(4):453–472, PMID: 25169849, https://doi.org/10.1016/j.cytogfr.2014.07.016.
73. De Stefano L, Pallavicini FB, Mauric E, Piccin V, Vismara EM, Montecucco C, et al. 2023. Tumor necrosis factor-α inhibitor-related autoimmune disorders. Autoimmun Rev 22(7):103332, PMID: 37062440, https://doi.org/10.1016/j.autrev.2023.103332.
74. Saraiva M, Vieira P, O'Garra A. 2020. Biology and therapeutic potential of interleukin-10. J Exp Med 217(1):e20190418, PMID: 31611251, https://doi.org/10.1084/jem.20190418.
75. Carlini V, Noonan DM, Abdalalem E, Goletti D, Sansone C, Calabrone L, et al. 2023. The multifaceted nature of IL-10: regulation, role in immunological homeostasis and its relevance to cancer, COVID-19 and post-COVID conditions. Front Immunol 14:1161067, PMID: 37359549, https://doi.org/10.3389/fimmu.2023.1161067.
76. Zhang Q, Zheng S, Shi X, Luo C, Huang W, Lin H, et al. 2023. Neurodevelopmental toxicity of organophosphate flame retardant triphenyl phosphate (TPhP) on zebrafish (*Danio rerio*) at different life stages. Environ Int 172:107745, PMID: 36657258, https://doi.org/10.1016/j.envint.2023.107745.
77. Lyons D, Guy A, Clarke J. 2003. Monitoring neural progenitor fate through multiple rounds of division in an intact vertebrate brain. Development 130(15):3427–3436, PMID: 12810590, https://doi.org/10.1242/dev.00569.
78. Addison M, Xu Q, Cayuso J, Wilkinson D. 2018. Cell identity switching regulated by retinoic acid signaling maintains homogeneous segments in the hindbrain. Dev Cell 45(5):606–620.e603, PMID: 29731343, https://doi.org/10.1016/j.devcel.2018.04.003.
79. Liu J, Jiao L, Zhong X, Yao W, Du K, Lu S, et al. 2022. Platelet activating factor receptor exaggerates microglia-mediated microenvironment by IL10-STAT3 signaling: a novel potential biomarker and target for diagnosis and treatment of Alzheimer's disease. Front Aging Neurosci 14:856628, PMID: 35572136, https://doi.org/10.3389/fnagi.2022.856628.
80. Gassmann M, Bettler B. 2012. Regulation of neuronal gaba(b) receptor functions by subunit composition. Nat Rev Neurosci 13(6):380–394, PMID: 22595784, https://doi.org/10.1038/nrn3249.
81. Antonellis A, Dennis MY, Burzynski G, Huynh J, Maduro V, Hodonsky CJ, et al. 2010. A rare myelin protein zero (MPZ) variant alters enhancer activity in vitro and in vivo. PLoS One 5(12):e14346, PMID: 21179557, https://doi.org/10.1371/journal.pone.0014346.
82. Peretyazhko TS, Zhang Q, Colvin VL. 2014. Size-controlled dissolution of silver nanoparticles at neutral and acidic pH conditions: kinetics and size changes. Environ Sci Technol 48(20):11954–11961, PMID: 25265014, https://doi.org/10.1021/es5023202.
83. Jin T, Zhang Y, Botchway B, Zhang J, Fan R, Zhang Y, et al. 2022. Curcumin can improve parkinson's disease via activating BDNF/PI3k/Akt signaling pathways. Food Chem Toxicol 164:113091, PMID: 35526734, https://doi.org/10.1016/j.fct.2022.113091.
84. ELBini-Dhouib I, Doghri R, Ellefi A, Degrach I, Srairi-Abid N, Gati A. 2021. Curcumin attenuated neurotoxicity in sporadic animal model of Alzheimer's disease. Molecules 26(10):3011, PMID: 34070220, https://doi.org/10.3390/molecules26103011.
85. Yang S, Zhou M, Chen X, Hu L, Xu Y, Fu W, et al. 2022. A comparative review of microplastics in lake systems from different countries and regions. Chemosphere 286(pt 2):131806, PMID: 34426137, https://doi.org/10.1016/j.chemosphere.2021.131806.
86. Badreddine B, Marc M, François O, Nikolaos M, Hrissi KK, Philippe B, et al. 2023. Extruded polystyrene microplastics as a source of brominated flame retardant additives in the marine environment: long-term field and laboratory experiments. Environ Int 172(0):107797, PMID: 36773563, https://doi.org/10.1016/j.envint.2023.107797.
87. Lee YK, Murphy KR, Hur J. 2020. Fluorescence signatures of dissolved organic matter leached from microplastics: polymers and additives. Environ Sci Technol 54(19):11905–11914, PMID: 32852946, https://doi.org/10.1021/acs.est.0c00942.